ANL-6452

ANL-6452

Argonne National Laboratory

# LECTURE NOTES ON IN-CORE INSTRUMENTATION FOR THE MEASUREMENT OF HYDRODYNAMIC PARAMETERS IN WATER-COOLED REACTORS

by

Glenn F. Popper

ANL-6452
Instruments
(TID-4500, 16th Ed.,
Amended)
AEC Research and
Development Report

ARGONNE NATIONAL LABORATORY
9700 South Cass Avenue
Argonne, Illinois

# LECTURE NOTES ON IN-CORE INSTRUMENTATION FOR THE MEASUREMENT OF HYDRODYNAMIC PARAMETERS IN WATER-COOLED REACTORS

by

Glenn F. Popper

Reactor Engineering Division

Presented at the Advanced Course on In-Core
Instrumentation for Water Cooled Reactors
Netherlands-Norwegian Reactor School
Kjeller, Norway

August 21 to September 1, 1961

November 1961

Operated by The University of Chicago
under
Contract W-31-109-eng-38

TABLE OF CONTENTS

# LIST OF FIGURES

## LIST OF FIGURES

## LIST OF FIGURES



## TABLE

# LECTURE NOTES ON IN-CORE INSTRUMENTATION FOR THE MEASUREMENT OF HYDRODYNAMIC PARAMETERS IN WATER-COOLED REACTORS

by

Glenn F. Popper

## I. INTRODUCTION

To begin with and to help clarify the type of instrumentation being discussed in this series of lectures, a definition of the term "in-core instrumentation" should be given. The term usually refers to any instrument system used to measure and record or indicate any parameter within the core of a nuclear reactor or within the pressure vessel that contains the core.

One may then ask, why is this "in-core instrumentation" needed? Instrumentation in the core of a nuclear reactor is necessary to gain a better understanding of reactor behavior. The information obtained from the measurement of core parameters has several valuable applications. First, the information obtained will be used to check the validity of reactor performance calculations. These reactor performance calculation techniques are reported in the literature.[1,2] Second, this information will be used to help evaluate the stability of the reactor by providing a direct measurement of a portion of the power-to-reactivity feedback transfer function. Further information on the dynamic behavior of reactors can also be found in the literature.[3,4] And third, this information may be used to extrapolate the reactor performance to higher power operation and, hence, to provide information to design improved and more efficient cores.

---

[1] Flinn, W. S., and Petrick, M., Performance and Potential of Natural Circulation Boiling Reactors, ANL-5720 (1957).

[2] Lottes, P. A., Petrick, M., and Marchaterre, J. F., Lecture Notes on Heat Extraction from Boiling Water Power Reactors, ANL-6063 (1959).

[3] DeShong, J. A., Jr., and Lipinski, W. C., Analyses of Experimental Power-Reactivity Feedback Transfer Functions for a Natural Circulation Boiling Water Reactor, ANL-5850 (1958).

[4] Akcasu, A. Ziya, Theoretical Feedback Analysis in Boiling Water Reactors, ANL-6221 (1960).

What are some of the problems that must be solved before it will be possible to make these reactor core parameter measurements? First, instrumentation capable of effectively measuring pressures, temperatures, flow rates, steam void fractions, steam-water interface level, and neutron and gamma fluxes within the reactor core during static, dynamic, and transient operation must be developed. These instruments must be able to withstand the severe environment of nuclear radiation, high temperature, and high pressure within the reactor core and vessel. One of the nuclear effects which must be considered is the damage to materials by neutron bombardment. This tends to limit the life of instruments used in the core of a reactor. Another is the damage and heating produced by gamma emission. These nuclear factors limit the choice of materials that can be used for these instruments. This is particularly true when one considers the rather poor electrical characteristics exhibited by most insulating materials after short exposures to nuclear radiation.

The instruments must be small enough to be used with the standard reactor fuel assemblies. They also must not alter, to any great extent, the parameters which they are measuring. Means must be found to bring the instrument signals out of the reactor vessel without interfering greatly with normal fuel-handling procedures. It also appears desirable to group the instrumentation in subassemblies that may be moved to many locations within the core. This grouping of the instruments will allow one to extract the maximum amount of information from the reactor with the minimum investment in instrumentation.

What reactor hydrodynamic parameters must be measured? The parameters that must be measured depend on the type of reactor being instrumented. For a natural-circulation boiling water reactor, such as is the Experimental Boiling Water Reactor (EBWR), the following hydrodynamic parameters are of interest and should be measured:

1. recirculation water flow rate in the downcomer;
2. inlet water velocity to the reactor fuel assembly;
3. exit steam void fraction of the reactor fuel assembly;
4. fuel plate heat flux and power generation;
5. steam void fractions in the riser above the core;
6. steam entrainment and void fractions in the downcomer;
7. water carryover into the steam line;
8. steam-water interface level above the core;
9. system pressure noise.

Instruments which will measure all of these parameters will be installed in the core and vessel of EBWR.

It should now be stated that the major portion of this lecture material will concern the techniques and instruments developed for use in the EBWR. Therefore, a brief description of this plant will be given, and the

in-core instruments will be shown positioned in the core and vessel. The EBWR is a complete, direct-cycle boiling water reactor power plant which can produce 5,000 kw of electricity from reactor steam at 41.8 atm. This electricity is fed into the Argonne National Laboratory distribution system. The reactor fuel is a mixture of natural, slightly enriched, and highly enriched uranium. Light water serves as a moderator and coolant. The reactor is designed to be cooled by boiling heat transfer to water circulating through the core by natural convection. A more detailed description of this plant can be found in the literature.[5]

Power generation itself is not the primary objective in the EBWR plant. The EBWR is primarily an experimental plant intended to provide as much information as possible for future use in designing larger plants. A part of this experimental program includes the measurement of the hydrodynamic parameters of the core. Figure I-1 shows a schematic view of the reactor vessel and the planned positions of the in-core or "in vessel" measuring instruments. A Pitot tube (A) and 2 Stauschiebe tubes (B) are placed in the downcomer to measure the recirculation flow rate of the reactor water. Static pressure taps (C) in the downcomer and riser will measure the mean mixture density at these points, from which the void fractions can be calculated. Pressure transducers (D) in the steam zone and downcomer will measure the pressure noise from which reactor stability will be studied. Pressure transducers (E), external to the core, will determine the steam-water interface level. Several instrumented fuel assemblies will also be installed in the core (see Figure I-2). Thermocouples (F) are placed at the inlet of a fuel assembly and in the steam zone to measure the inlet subcooling from which the water recirculation flow rate or steam entrainment in the downcomer can be calculated. Turbine flowmeters (G), placed at the inlet and exit of a fuel assembly, will measure the inlet and exit liquid velocities. From these two measurements and a knowledge of the inlet subcooling and exit quality, the steam void fraction at the fuel assembly exit can be calculated. Ionization chambers (H) in the fuel assembly channels will measure the thermal and epithermal flux from which the steam void fraction at that point can be calculated. Thermocouples in a special fuel plate (I) of one of these assemblies, will measure the centerline fuel temperature from which the heat flux of and power generated in the fuel plate can be determined.

All of these instruments and techniques, along with others being considered for other reactor types, will be described fully in later sections, and this brief description is presented now only to give an overall picture of the measurements that will be made in the core of EBWR.

---

[5] Experimental Boiling Water Reactor, ANL-5607 (1957).

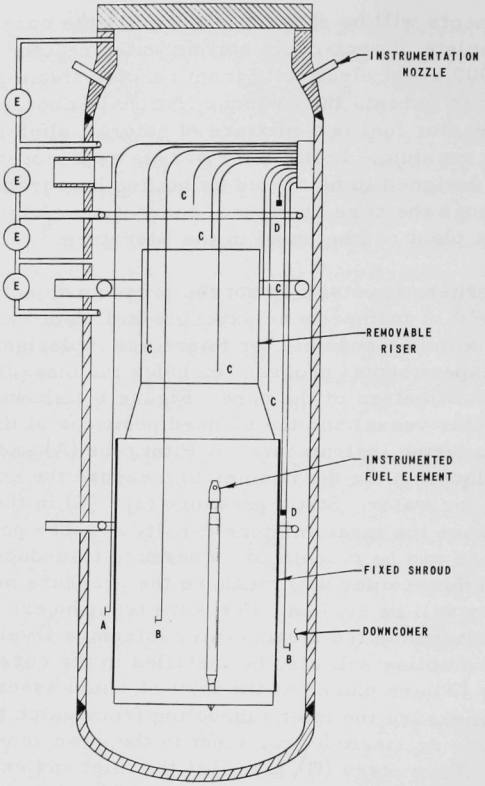


Fig. I-1

EBWR Vessel Showing In-Core Instrumentation

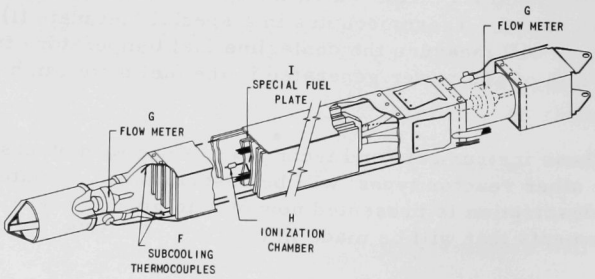


Fig. I-2

Instrumented Fuel Assembly for EBWR

# II. PRESSURE MEASUREMENTS

## A. Introduction

Normally, the system pressure of a water-cooled reactor is measured by using transducers which are connected to a water column some distance away from the core. The differential pressures developed across flow nozzles and orifices are also measured in a similar manner. When pressure measurements are made in this manner, conventional transducers can be used and the problems associated with in-core instruments are of little concern. If the system pressure of a reactor can be measured so easily, one may then ask why are in-core pressure measurements needed at all. Several applications are apparent at the present time and others will develop over the years.

DeShong has shown[6] that the random variations appearing in the flux of a boiling water reactor are related to the pressure-dependent portions of the theoretical model and that the so-called "boiling noise" in a reactor originates in the random variation of the rate of steam generation. He has also shown that the steam-water interlayer can be considered a "white" noise source over a frequency range from 0.7 to 20 radians/sec. This range includes the frequency spectrum of interest when studying reactor stability. Therefore, if a "white" noise source exists as an input signal to the pressure vessel steam dynamics system, the measured pressure noise signal or output should yield its transfer function. The pressure signal that is used for this analysis must, however, be unaltered by the effects of connecting lines and must, therefore, be obtained inside the reactor vessel.

The measurement of the pressure drop across reactor fuel elements is also an important application. This measurement would help analyze the performance of reactor fuel assemblies and would help set criteria for the design of more efficient fuel elements.

We shall now investigate several pressure transducers which show great promise of being adapted to in-core applications.

## B. Unbonded Strain Gage Pressure Transducers

The unbonded strain gage pressure transducer exhibits desirable features which make it suitable for in-core applications. It is a small instrument and is a transducer capable of withstanding the severe environment

---

[6] DeShong, J. A., Jr., Flux, Reactivity, Steam Void, and Steam-Water Interlayer Noise Spectrums in the EBWR, Reactor Sci. 10, 147-156 (Sept 1959).

within the reactor vessel. Its compatibility with corrosive media is excellent and it is highly accurate. It is also suitable for both static and dynamic measurements.

Strain gage transducers[7] are electromechanical devices which translate minute mechanical displacements of a diaphragm into proportional resistance changes of a Wheatstone bridge. The transducer is constructed so that it is electrically and mechanically symmetrical. In the center of a stationary frame (F), an armature (A) is supported rigidly in the plane perpendicular to the longitudinal axis. Wound between rigid insulators mounted in the frame and armature are four filaments, "G," "H," "I," and "J," of strain-sensitive resistance wire, as shown in Figure II-1a. These four resistance elements are bridge connected internally as shown in Figure II-1b.

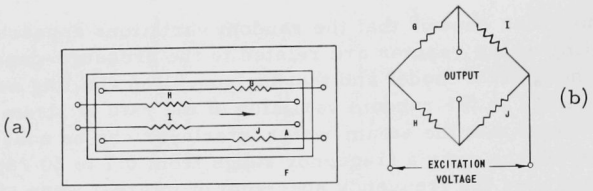


Fig. II-1

(a) Transducer Mechanical Arrangement
(b) Bridge Connection

As the armature is caused to move longitudinally to the right, for instance, by an external force (see Figure II-1a), elements "H" and "I" increase in length while elements "G" and "J" decrease in length. The change in the resistance of these filaments is proportional to the change in their length. This resistance change alters the electrical balance of the bridge and produces an electric signal in the output circuit. Sufficient initial tension is applied to the strain-sensitive resistance wires during assembly to keep them under some residual tension when the armature is in either extreme position. The armature is usually limited mechanically at either extreme to protect the wires from excessive overload.

This transducer becomes a pressure pickup when a metallic diaphragm is connected to the armature. The transducer now measures the displacement of the center of the diaphragm, which is proportional to the applied pressure. The strain-sensitive wires will contribute comparatively little to the stiffness of the moving system. This effect is important when the transducers are used for dynamic measurements.

---

[7] Descriptions taken from Stathum Instrument Notes.

One of the parameters of primary interest to the user of a pressure transducer is its natural or resonant frequency. The resonant frequency of any network is that frequency at which the driving source sees a pure resistive load. The natural frequency of the pressure transducer is given by

$$\omega_n = \sqrt{K/M} \qquad \text{(II.1)}$$

where $\omega_n$ is the natural frequency, K is the spring constant, and M is the mass of the moving system. The damping of the transducer has nothing to do with the natural frequency, but does affect the period at which oscillations will occur.

Pressure transducers are not normally damped by any means other than internal friction and have rather high natural frequencies in air around 20 kc. Some damping will be introduced by the fluid on which the measurements are being made. However, as far as the amplitude response is concerned, the response will be flat up to about 0.2 of the natural frequency, even though the damping is negligible. In estimating the frequency response of a system, the length and size of the connecting tubing and the effect of the cavity volume is usually the controlling factor.

By applying pressure to one side of the diaphragm and venting the other to the atmosphere, gage pressure is measured. If the transducer is evacuated, absolute pressure is measured. Another modification can be made so as to provide two pressure connections, one to each side of the diaphragm, for the measurement of differential pressure.

As the electric circuit of the transducer is a complete and balanced bridge, the power supply requirement is generally quite simple. A dry battery is usually adequate, although for in-core use an alternating current or a carrier system may be needed. The reason for using a carrier or a-c system, when making in-core measurements is that very often the connecting cable itself generates a direct-current signal when exposed to nuclear radiation. This signal could be interpreted as a pressure change if direct current was used as the exciting source. A carrier or a-c system will reject this extraneous d-c signal.

Ambient temperature variations are one of the major sources of error in this instrument. These errors are of two kinds. First, the zero setting may shift with temperature because of unequal mechanical expansion of instrument members. Second, the calibration factor, span, or sensitivity, as it is variously called, may also vary with the ambient temperature. This could be caused by the changes in the modulus of elasticity of the gage members. As the ambient temperature of a reactor vessel may vary from 20 to above 300°C, these errors must be reduced to a point where they are negligible.

To minimize zero shifts with temperature, the first requirement is that the differential expansion of the mechanical system must nearly balance out. This expansion cannot normally be eliminated but can be reduced until the total effect is a small fraction of the full-scale output of the transducer over a moderate temperature range. The remaining zero-shift error can be compensated for electrically.

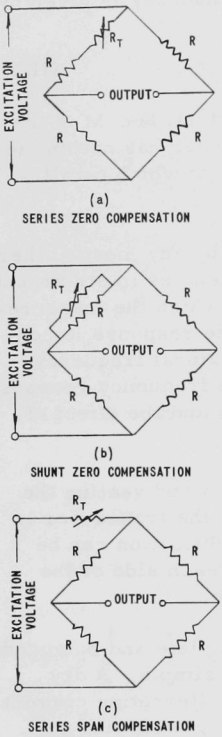


Fig. II-2
Temperature Compensation Circuits

This electrical compensation can be accomplished by connecting a temperature-sensitive resistor, $R_T$, in series with one arm of the bridge, as shown in Figure II-2a. Since most wire resistor materials have positive temperature coefficients, the temperature-sensitive resistor is placed in the arm which would cause an output change in the opposite direction to the zero shift with increasing temperature.

A second method of zero compensation is known as shunt compensation. In this case, a temperature-sensitive resistor is connected across appropriate corners of the bridge, as shown in Figure II-2b. When using this type of compensation, the temperature-sensitive network is placed across an arm which will produce a zero shift in the same direction as the drift with decreasing temperature.

Each of these methods of temperature compensation has a slight effect on the span and, hence, the calibration. The calibration of a pressure transducer should always be carried out after both zero and span compensations are made.

The second cause of errors in pressure transducers are the variations in sensitivity with temperature. These changes in span are usually caused from the changes in the modulus of elasticity of the materials. Regardless of the source of error, transducers usually give a larger output with increasing temperature so that the thermal coefficient of sensitivity is positive. Electrical compensation must also be used to correct for these temperature effects.

Although there are a variety of methods which can be used for this compensation, the most common is the series span method. In this the voltage to the transducer is held constant and the current to the bridge is made to vary automatically by placing a temperature-sensitive resistor in series with the transducer input, as shown in Figure II-2c. With this varying current, the span will remain fairly independent of temperature.

Unbonded strain gage transducers have been proven to be unaffected by radiation[8] and, hence, they will be used to measure the pressure noise in the vessel of the Experimental Boiling Water Reactor. Figure II-3 shows a drawing of the transducers supplied by Consolidated Electrodynamic Corporation.

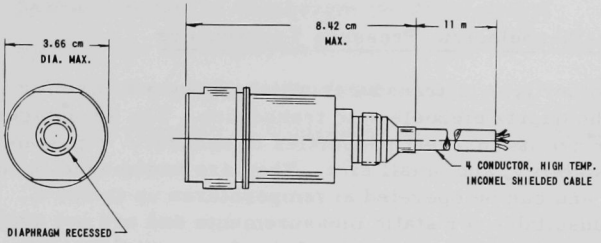


Fig. II-3

In-Core Pressure Transducer

All of the electrical compensations are provided by the transducer manufacturer. Listed below are the more important specifications of these transducers.

1. Environmental Specifications

   1.1 Compensated Temperature Range: -54°C to 260°C.

   1.2 Zero Shift with Temperature: +0.005% of full range/°C.

   1.3 Thermal Coefficient of Sensitivity: +0.05% of full range/°C.

   1.4 Neutron Flux: To withstand $4 \times 10^{13}$ nv.

   1.5 Gamma Flux: To withstand $1 \times 10^{9}$ r/hr.

2. Physical Specifications

   2.1 Insulation Resistance: 10 megohms minimum at 45 volts d-c over compensated temperature range.

   2.2 Cable: 10 meters in length, outside diameter not larger than 0.8 cm.

3. Materials

   3.1 Structural, External: Type 304 stainless steel.

   3.2 Structural, Internal: Insulators will be nonorganic low boron type.

---

[8]Harris, S. P., and Bumpus, C. F., Jr., Pressure and Temperature Instrumentation for Dynamic Measurements in the KEWB Program, NAA-SR-4709.

3.3 Cable Insulation: Aluminum oxide.

3.4 Cable Sheath: Inconel.

3.5 All materials to be operative in nuclear radiation environment.

C. Quartz-Piezoelectric Pressure Transducers

Another type of transducer which shows promise for in-core application is the quartz piezoelectric transducer. The advantages of this transducer are its inherent properties of accuracy, repeatability, high strength, stability, and small size. They are undamaged by nuclear radiation doses and can be operated at temperatures up to 300°C. They are, however, unsuitable for static measurements and are not available for measuring differential pressures. It is also very difficult to reduce the effects from radiation-induced signals in the connecting cable.

This instrument is also an electromechanical transducer. Pressure applied on the diaphragm end of the transducer stresses two quartz crystals which generate an electrostatic charge proportional to the applied pressures. An electrostatic amplifier is then used to couple this transducer to the readout instrument.

Figure II-4 shows the actual and simplified equivalent circuits of a piezoelectric transducer.[9] The simplified circuit will be used for the purpose of explaining the transducer's behavior. The transducer can be thought of as a capacitor ($C_p$) which is also a coulomb generator generating a specific charge (q) across its electrodes. The voltage (E) out of the transducer is equal to

$$E = q/C_p \quad . \tag{II.2}$$

The simplified circuit shows that the transducer and the input impedance of any associated electronics are equivalent to a high-pass filter with a low-frequency cutoff point determined by the combined RC time constant of the amplifier and transducer system, and this is the reason that this type of transducer is not suitable for static measurements.

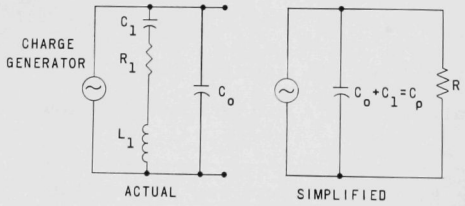


Fig. II-4

Equivalent Circuit of Piezoelectric Transducer

[9] Mason, W. P., Piezoelectric Crystals and Their Application To Ultrasonics, D. Van Nostrand Company.

D. Nomenclature

| | |
|---|---|
| $E$ | Output voltage (volts) |
| $C_p$ | Capacitance of transducer and cable (farads) |
| $K$ | Spring constant of diaphragm (Newton/meter) |
| $M$ | Mass of the moving system (kilogram) |
| $q$ | Specific charge generated (coulombs) |
| $\omega_n$ | Natural frequency of transducer in air (radians/second) |

# III. WATER FLOW RATES

## A. Introduction

Before discussing the instruments that could be used to measure water flow rates, several of the specifications that must be placed on these flow-measuring instruments should be related. These instruments for use in the EBWR must be capable of operating in an environment having temperatures as high as 252°C, pressures as high as 81.8 atm, and neutron fluxes as high as $10^{14}$nv. They must be small enough to fit within the outside dimensions of a standard fuel assembly and must not substantially reduce the flow through the fuel assembly. The output signal should preferably be electrical so that it can be easily brought out of the reactor vessel.

A review of available flow instruments was made to see which standard flowmeters fitted these specifications. Differential-pressure-producing, variable area, and turbine-type flowmeters were thought to be the most promising. The hot wire anemometer and magnetic flowmeter were also considered. Heat balance techniques were also investigated.

## B. Heat Balance Techniques

One way that the recirculation water flow rate in a "pot" type boiling water reactor can be measured directly is by placing a differential-pressure-producing device in the downcomer. The recirculation water flow rate through the core can also be determined by a heat balance method if the steam entrainment in the downcomer is zero. Essentially, this flow is determined if the difference between the outlet and inlet temperature of the reactor core is measured, along with some of the usual plant parameters (as feedwater flow rate and temperature, system pressure, ion exchange flow rate and temperature, and total steam flow rate).

The EBWR flow system is shown schematically in Figure III-1; it has been assumed that all of the energy produced, $Q_t$, is absorbed by the water in the core, and none is transferred to the water in the downcomer. Heat losses from the reactor are considered negligible, and it is further assumed that $h_{Iout} = h_f$ and $h_m = h_{ml} + h_{Iin}$.

The following parameters are defined:

$$x_e = W_s/W_t$$

is the average core exit quality;

$$x_D = W_{sz}/W_t$$

is the steam entrainment in the downcomer.

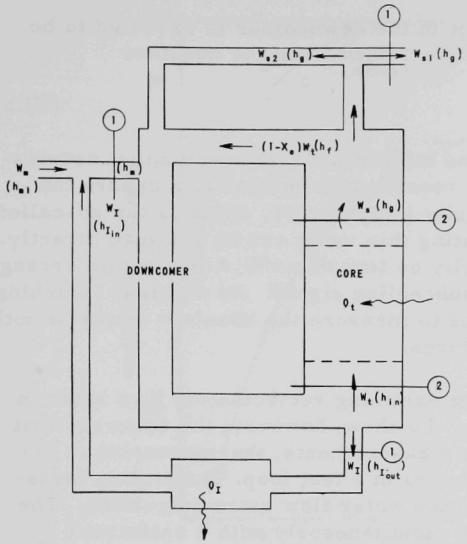


Fig. III-1

EBWR Schematic Flow Diagram

From an energy balance on the system within boundary (1),

$$Q_t = W_{s1}h_g - W_m h_m + W_I(h_f - h_m) \quad . \tag{III.1}$$

Then, from an energy balance on boundary (2),

$$Q_t = W_t(x_e h_{fg} + h_f - h_{in}) \quad . \tag{III.2}$$

Then, combining Equations (III.1) and (III.2), the recirculation water flow rate is

$$W_t = \frac{(W_m + W_I)(h_f - h_m)}{(h_f - h_{in}) + x_D h_{fg}} \quad . \tag{III.3}$$

The feedwater flow rate $W_m$, ion exchange flow rate $W_I$, feedwater enthalpy $h_m$, and pressure are known from plant measurements. Steam entrainment in the downcomer, $x_D$, is assumed to be zero. Equation (III.3) then reduces to

$$W_t = \frac{(W_m + W_I)(h_f - h_m)}{h_f - h_{in}} \quad , \tag{III.4}$$

and, therefore, only the reactor subcooling need be measured to calculate the recirculation water flow rate. How valid the approximation that the steam entrainment in the downcomer is zero is discussed later.

Since the steam entrainment in the downcomer is assumed to be zero, the core exit quality can be determined from the equation

$$x_e = W_m/W_t \quad . \tag{III.5}$$

Thermocouples placed at the inlet of several reactor fuel assemblies and in the steam dome of the reactor will be used to measure the difference between the outlet and inlet temperature, which is the so-called reactor subcooling; a signal indicating this value can be obtained directly. Because the subcooling will normally be less than 6°C, a thermopile arrangement will be used to amplify this subcooling signal. An external switching arrangement also provides a means to measure the absolute values of both the inlet and steam dome temperatures.

Heat balance methods for determining recirculation flow rates in boiling systems are quite common. To show, however, the accuracy that would be expected from subcooling measurements, thermocouples of the type to be used in EBWR were installed in a test loop. Subcooling measurements were taken and recirculation water flow rates calculated. The water flow rate was also measured simultaneously with a calibrated turbine flowmeter. Figure III-2 shows the error plot obtained by comparing the two flow rates. From this figure, it can be seen that the expected accuracy of the heat balance method is about ± 10%.

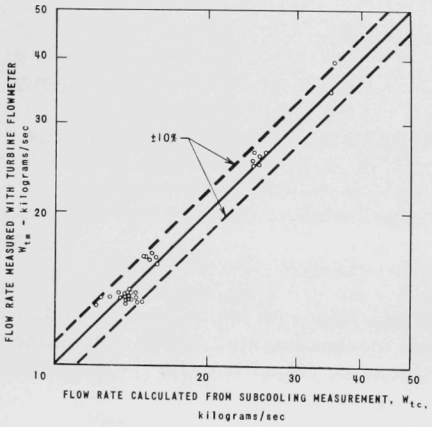


Fig. III-2

Error Plot of the Flow Rate Determined from Subcooling Measurements Compared to the Flow Rate Measured by a Calibrated Turbine Flowmeter

The recirculation flow rates of the EBWR have been determined using a heat balance method.[10] In both cases, the steam entrainment was assumed zero. Figure III-3 shows the data taken by Bernsen and by Sutherland.

[10] EBWR Test Reports, ANL-6229, pp. 293-303.

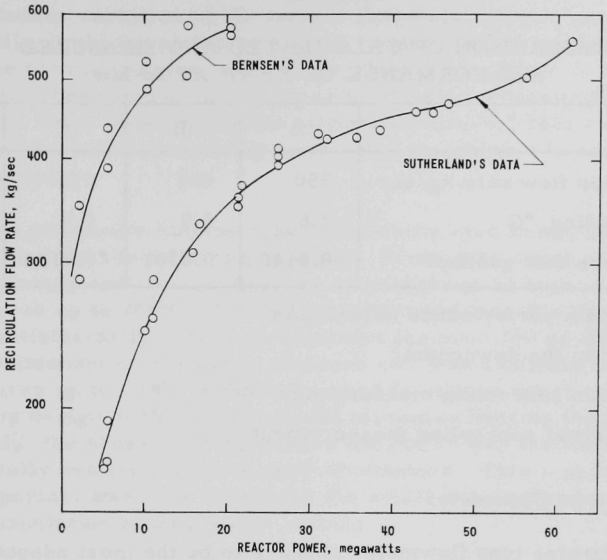


Fig. III-3

Recirculation Flow Rate at Various Reactor Powers and System Pressure of 41.8 Atmospheres

The recirculation water flow rates and average exit qualities have been calculated by Viskanta and Weatherhead,[11] who assumed zero steam voids and about 12% average steam voids in the downcomer. The two calculated recirculation flow rates differed by 30%, most of which was due to the presence of or absence of voids in the downcomer. Tests run by Bernsen[12] indicated the possibility of such steam entrainment in the downcomer of EBWR, but this parameter was not investigated at that time. Table III-1 lists the calculated and measured values of recirculation flow rate, subcooling, and exit quality at a power of 20 Mw. It can be seen that the values listed vary radically, indicating the need for more refined measurements. If, for instance, a differential-pressure-producing device is placed in the downcomer, then the recirculation flow rate is determined directly and the heat balance will indicate the presence or absence of steam entrainment in the downcomer.

---

[11] Weatherhead, R. J., and Viskanta, R., EBWR Performance at 20 Mw, Personal Communication (May 1958).

[12] Bernsen, S. A., et al., Reactor Engineering Quarterly Report, Oct 1, 1954 through Dec 31, 1954, ANL-5371, p. 197.

Table III-1

COMPARISON OF CALCULATED AND MEASURED PERFORMANCE OF EBWR AT 20 Mw

| | A | B | C | D |
|---|---|---|---|---|
| Recirculation flow rate, kg/sec | 550 | 425 | 572 | 364 |
| Inlet subcooling, °C | 2.6 | 3.9 | 2.9 | 4.2 |
| Average core exit quality | 0.0140 | 0.0181 | 0.0134 | 0.0213 |

A. Optimum performance calculation

B. Voids in the downcomer

C. Bernsen subcooling measurement

D. Sutherland subcooling measurement

C. Turbine-type Flowmeter

The turbine type flowmeter appears to be the most adaptable instrument for in-core applications and was, therefore, selected to measure the reactor core inlet water velocity in the EBWR. A typical turbine-type flowmeter is shown in Figure III-4. It consists of a body, a turbine with a small two- or four-pole Alnico magnet cast into it, and a coil mounted on the body adjacent to the turbine.

When the liquid flows through the meter body, the turbine rotates at a speed determined by the velocity of the liquid passing the rotor blades and the blade angle. As the magnets rotate, an a-c voltage is induced in the coil. The frequency of this voltage is equal to the speed of the turbine or twice the speed, depending upon the number of poles to the magnet. This a-c voltage is connected to the measuring instrument, in which it is converted to a direct current proportional to the input frequency.

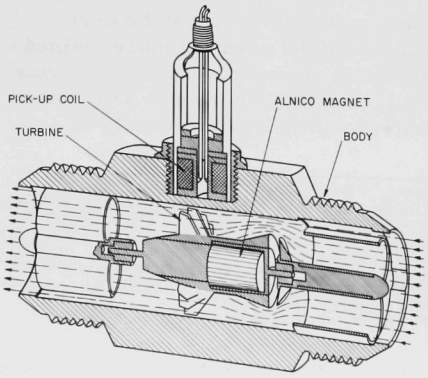


Fig. III-4

Electronic Flow Sensing Element

Another variation of the turbine flowmeter uses a variable-reluctance type of coil. In this case the turbine is constructed of a magnetic material and, as the turbine rotates, each blade produces a change in the impedance of the coil. These impedance changes produce a frequency signal which is equal to the rotor speed times the number of blades. This a-c signal is then also connected to the measuring instrument, in which it is converted to a direct current.

The particular turbine-type flowmeters used in our application were selected for the following reasons. First, long-term performance data had already been run at Argonne at pressures as high as 69 atm and temperatures up to 260°C. These tests indicated that this flowmeter will perform satisfactorily in this environment for over 250 hr without the need of maintenance. Second, a standard coil was available for use at temperatures up to 538°C without the need for air or water cooling. Third, the floating design of the turbine would minimize bearing friction and wear. And, finally, the pressure drop across the meter was the lowest of all commercially available turbine-type flowmeters. This last item is particularly important when one considers the small driving head available in a natural-circulation boiling water reactor.

In order to be able to use the turbine flowmeter in the reactor to measure the inlet water velocity, several modifications to the standard high-temperature meters were necessary. First, the relatively large standard high-temperature coil had to be reduced in size so that the entire flowmeter and coil would be smaller than the outside dimensions of the fuel assembly. The electrical leads had to be an integral part of the coil assembly so that the coil and leads would withstand the pressure and temperature in the reactor vessel. And, last, the entire flowmeter had to be constructed of materials that would be compatible with the nuclear environment of the core. Figure III-5 shows a drawing of a standard high-temperature coil. This coil is about 6.0 cm in height and screws into the meter body. It is not designed to be immersed in high-temperature water and is not sealed to contain the system pressure. The electrical lead is only about 30 cm long and is also not immersible in water. Figure III-6 shows the coil as redesigned for use on the in-core flowmeters. This coil is only 2.54 cm in height and affixes to the meter body by means of a flange. The coil is wound with a ceramic-insulated wire. The cable, which is made long enough to extend out of the reactor vessel, is welded to the coil assembly. The two nickel wires that are enclosed in the Inconel sheath and insulated by aluminum oxide are

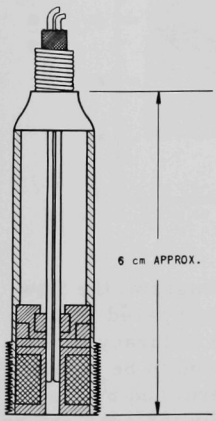


Fig. III-5
Cutaway of Standard High Temperature Pickup Coil

then welded to the ends of the coil. The entire assembly is potted with a ceramic cement and a plug is then welded to the coil housing to make it pressure tight.

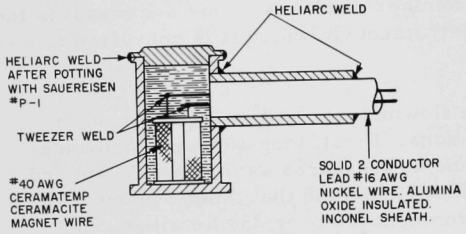


Fig. III-6

Cutaway of Redesigned High Temperature Pickup Coil

The flowmeter that is being used to measure the inlet water velocity in the EBWR is shown in Figure III-7. It is manufactured by the Potter Aeronautical Company. The stainless steel body of this flowmeter was specially designed so that it would replace the nose piece of a standard EBWR fuel assembly. The body and coil do not exceed the approximately 10 cm by 10 cm dimensions of the fuel assembly. The guide bearings and thrust stops are made of graphitar No. 30 and sapphire, respectively, and the magnets are of Alnico.

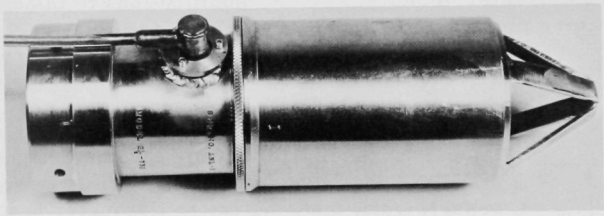

Fig. III-7

Inlet Turbine Flowmeter

During a portion of an out-of-pile experimental program, the flow rate measured by a turbine flowmeter was continuously compared with the flow rate determined by a calibrated venturi meter. The accuracy of the turbine flowmeter, using factory calibration data, was found to be within ± 1% and repeatable to within ± 0.5% of the flow rate determined by the venturi meter. This flowmeter has operated satisfactorily for over 350 hr in an environment of 252°C and 41.8 atm.

In order to be able to analyze the dynamic characteristics of a flow system, the frequency response of the overall flow-measuring system must be known. The frequency response representing the coupling between

the flowmeter turbine and the fluid is known to be flat to about 10 cps, but depends on the meter size and flow rate.[13]

The frequency response of the frequency converter remained to be determined. A frequency-modulated carrier was needed for this purpose. The frequency spectrum of interest is from about 0.1 to 10 cps. A standard instrument capable of producing this type of signal was not available and one had to be improvised. The improvised instrument consisted of an audio oscillator equipped with a mechanical drive mechanism that would sinusoidally vary the frequency about a base frequency. Using this apparatus, the transfer function of the converter was determined. The frequency response was found to be flat to 5 cps, the 3-db point, as shown in Figure III-8. The frequency response of the overall flow-measuring system is, therefore, presently limited by the converter. Methods of increasing the response of the overall system are now being studied.

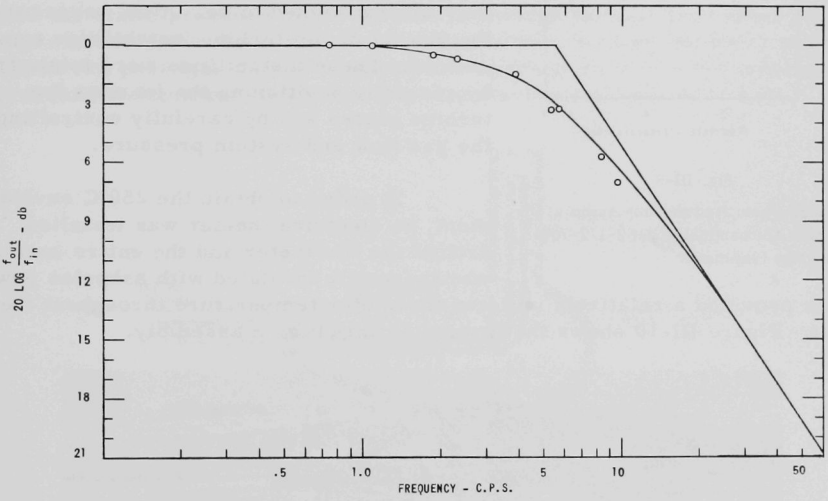


Fig. III-8

Frequency Response of Frequency Converter

In order to be able to predict accurately the hydrodynamic performance of a fuel assembly which is installed in a natural-circulation system, the single-phase pressure drop across the turbine flowmeters must be exactly known. The single-phase pressure drop can usually be obtained from the flowmeter manufacturer. However, experience has shown that these pressure drops apply only to meters of standard construction. If the meter body configuration is changed, the actual pressure drop across the meter must be measured. Figure III-9 shows a typical deviation from the manufacturer's values of single-phase pressure drop.

[13]Grey, J. Transient Response of the Turbine Flowmeter, Jet Propulsion (Feb 1956).

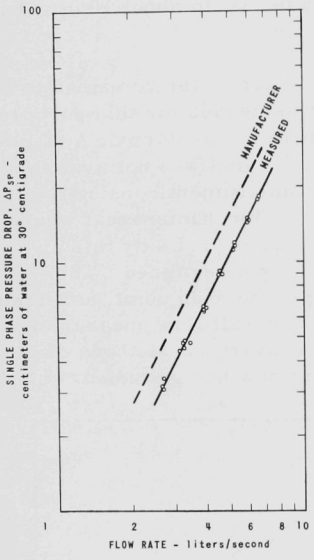


Fig. III-9

Single-Phase Pressure Drop Across a Potter Aeronautical Model 2-1/2-760 Turbine Flowmeter

A small-size turbine flowmeter and a pickup coil constructed of material identical to the type being used on the instrumented fuel assemblies was irradiated in the CP-5 reactor. The main purpose of this irradiation test was to observe the performance of the pickup coil and the Alnico magnets, which generate the output signal, in a high temperature, nuclear environment.

Because of limitations imposed by the irradiation facility, a carbon dioxide gas jet had to be used to drive the turbine of the flowmeter under test. This gas jet drive was undesirable because the turbine bearings would not be lubricated with water as they were designed to be. Also, because of the gas jet drive, turbine instabilities were noticed. These instabilities were minimized by carefully positioning the jet near the turbine blades and by carefully controlling the gas flow and system pressure.

In order to obtain the 250°C environment, an electrical heater was installed around the flowmeter and the entire assembly was thermally insulated with asbestos powder. This provided a relatively uniform flowmeter temperature throughout the test. Figure III-10 shows the flowmeter irradiation assembly.

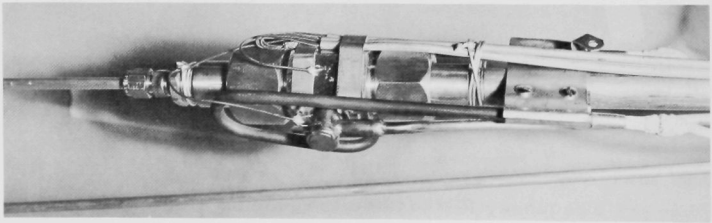

Fig. III-10

Turbine Flowmeter Irradiation Assembly

After 1,000 hr of operation at 250°C in a thermal neutron flux of approximately $3.5 \times 10^9$ nv, the test was terminated. This corresponds to an integrated flux of about $1.26 \times 10^{16}$ nvt. The output signal amplitude from the flowmeter was measured periodically throughout the test and was

found to be unaffected by this environment. The bearings also performed satisfactorily even without their normal water lubricant. Although the neutron flux at the flowmeter was approximately four decades lower than the flux expected in EBWR and was all thermal, the results obtained were added assurance that the flowmeter and pickup coil has an excellent chance of performing satisfactorily in the EBWR. A more detailed analysis of the pickup coil and bearing performance will be made when the flowmeter assembly can be visually examined and inspected.

D. Differential-pressure-producing Devices

The velocity of a fluid stream may be measured by using the effect of dynamic pressure. The most frequently used instrument is the so-called Pitot-static tube shown in Figure III-11. The wall of the Pitot tube portion of the probe is constructed in the form of an annular passage, in the outer surface of which the static-pressure holes are put. The dynamic pressure plus the static pressure of the stream is carried through the center passage, and only the static pressure is transmitted through the outer passage. These two passages may be connected to opposite ends of a differential pressure transmitter which will indicate the dynamic pressure $\Delta P$.

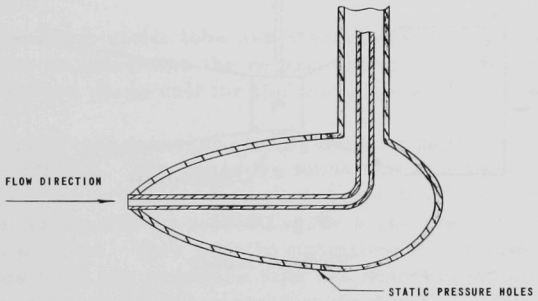


Fig. III-11

Simple Pitot-Static Tube

From Bernoulli's theorem,

$$V = 101.6 \sqrt{2g\Delta P/\rho} \quad . \tag{III.6}$$

With this type of instrument, interference and misalignment produce errors in the measurement. The errors in static and total pressure, however, tend to compensate each other, and this type of probe is less sensitive to misalignment than is the simple Pitot tube. Because of these interference effects, the probe must be calibrated, and Equation (III.6)

must be modified by a calibration coefficient such that

$$V = 101.6C \sqrt{2g\Delta P/\rho} \quad , \tag{III.7}$$

where C is a calibration coefficient.

The Venturi meter is another device which is widely used for measuring liquid velocities. This instrument consists of a tube constructed as shown in Figure III-12. It has an inlet section which is tapered, a short constant-diameter section called the throat, and a tapered outlet section. Again, from Bernoulli's equation,

$$V = 101.6 \sqrt{\frac{2g\Delta P}{(n^2 - 1)\rho}} \quad . \tag{III.8}$$

Pressure taps are placed at the inlet and throat of the meter and the differential pressure is measured by a pressure transmitter.

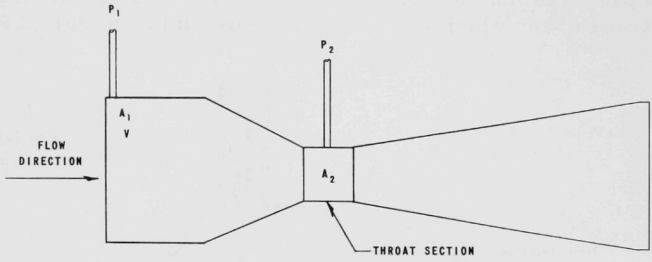


Fig. III-12

Venturi Meter

Again, for accurate results, the meter should be calibrated and a coefficient determined. This coefficient corrects for nonuniform velocity distribution and energy losses. Equation III.8 then becomes

$$V = 101.6\ K \sqrt{\frac{2g\Delta P}{(n^2 - 1)\rho}} \quad , \tag{III.9}$$

where K is a calibration coefficient.

The Stauscheibe tube, shown in Figure III-13, is a modification of the Pitot static tube. This probe is different only because of its configuration and higher calibration coefficient $\approx 1.5$. The Stauscheibe tube is also less sensitive to misalignment errors but, as in the case of the Pitot static tube, must be calibrated. The equations used to determine the velocity are, however, the same.

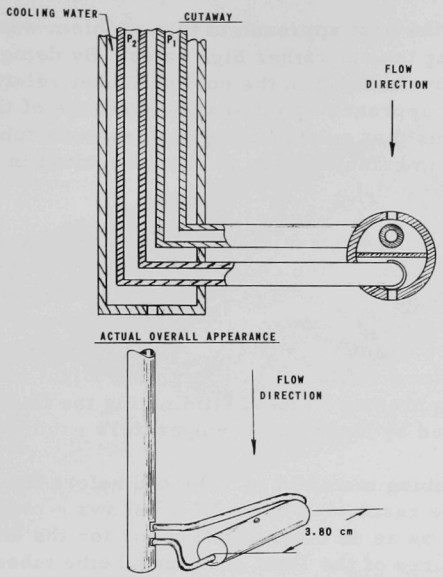


Fig. III-13

Stauscheibe Tube

Both the Pitot-static tube and Stauscheibe tube are being used at the present time to determine the recirculation flow rate in the EBWR downcomer. Future plans call for the installation of a Venturi meter.

Differential-pressure-producing devices appear to be ideally suited for in-core use. The pressure tubes that are used to transmit the pressure signals out of the reactor vessel are of a "concentric water-cooled" design and enable us to contain the high- and low-pressure taps in a single larger tube. This greatly simplifies the installation. The individual tubes from the pressure taps are mounted inside a larger tube carrying cooling water from a central connector box. This box is mounted on the inside wall of the reactor vessel above the core. The pressure taps are separated from the cooling water tube on the inside of the connector box and are led through the vessel penetration to a connector head. At this point, they are isolated from the reactor system and connected to differential pressure transducers. The electrical signals from the transducers are then transmitted to strip chart recorders mounted in a control room.

One problem that was encountered during our out-of-pile testing was the proper cooling of the pressure tubes as they pass up through the steam zone. If the tubes are not cooled properly, the water inside the pressure taps will reach the saturation temperature of the boiling system in which they are immersed. When this occurs, the saturated water can flash to steam as soon as head pressure in the tube becomes less than the system pressure outside the tube. This will essentially destroy the differential pressure signal.

It was originally felt that the best approach to this problem was to inject feedwater into the cooling tube at rather high rates. By doing this, a low temperature could be maintained in the cooling jacket relative to the system temperature. This approach was discarded because of the severe axial temperature gradients that existed along the pressure tubes. The inability to measure or even to calculate this gradient resulted in large errors in the pressure differentials.

The final approach to this problem was to use a very low rate of coolant water flow. By using this method, the cooling water nearly reached the saturation temperature of the system shortly after entering the cooling jacket, and remained at a fairly constant temperature over the length of the cooling tube. The temperature drops through the walls of the concentric tubes and the cooling water layer are sufficient to maintain a slight subcooling up the entire length of the pressure tubes, eliminating the flashing problem and the difficulties caused by large axial temperature gradients.

Figure III-14 shows the tubing manifold as it looked before the connector box was installed in the reactor. Figure III-15 shows a closeup of the connector head, which serves as an outer junction box for the differential pressure signals. Pictures of the Pitot and Stauscheibe tubes are unavailable at this time.

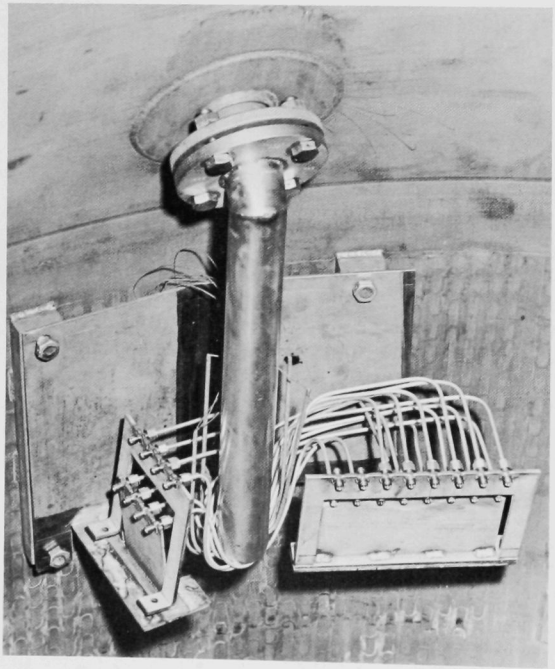

Fig. III-14

Close-up of
Tubing Manifold

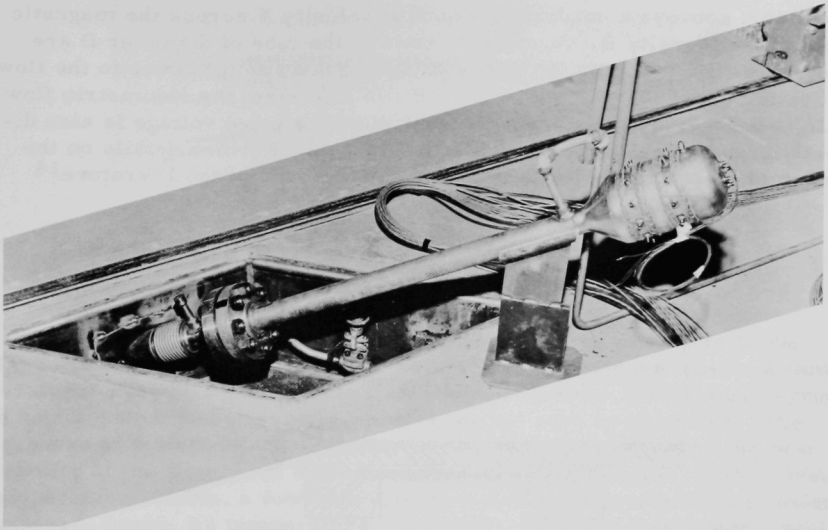

Fig. III-15

Connector Head

E. Electromagnetic Flowmeters

The electromagnetic flowmeter could also be used for measuring in-core flow rates. Some of the advantages of this type of instrument are obstructionless flow, hence no pressure loss, calibration unaffected by density or viscosity, linear flow signal, bi-directional measurement, and straightening vanes, piping runs, or purges not required. The major disadvantages of the flowmeter are its large size due to the coils and iron, which produce the magnetic field, and the selection of liner materials for the flow tube, which will withstand the high-temperature, nuclear radiation environment. The liner must also be noncorrosive to the flowing fluid, nonmagnetic so as not to affect the uniform magnetic field, and an electrical insulator to prevent the grounding of the flow signal.

The electromagnetic flowmeter operates as a simple a-c generator in which the flowing liquid is the armature and the electrodes act as brushes. Figure III-16 shows the essential parts of the primary element. Faraday's law of electromagnetic induction states that the movement of a conductor at right angles through a magnetic field produces a voltage in a plane mutually perpendicular to the field and to the direction of movement. An a-c electromagnet, consisting of two coils, produces a vertical flux. A nonmagnetic flow tube, whose inner surface is lined with a electrical

insulator, conveys a conducting liquid at velocity V across the magnetic field of flux density B. At opposite ends of the tube of diameter D are electrodes through the pipe wall, which detect a voltage E due to the flow, which is equal to BVD. Since, for a given pipe size, the volumetric flow rate is dependent solely on flow velocity, this induced voltage is also directly proportional to the volumetric flow rate. Further details on the design of electromagnetic flowmeters can be found in the literature.[14]

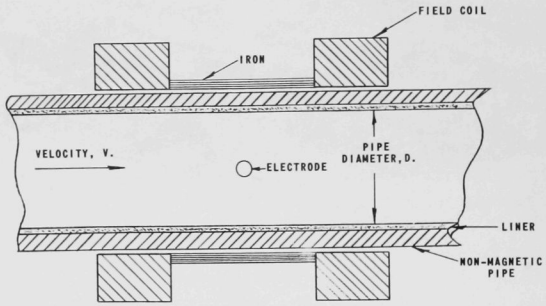


Fig. III-16

Electromagnetic Flowmeter

There has been considerable progress in developing suitable liner materials[15] and high-temperature, radiation-resistant insulated wire is available for the field coils. It appears, then, that the major problem in adapting the electromagnetic flowmeter for in-core use is the reduction in size of the coils used to generate the magnetic field. If this design problem could be solved, the electromagnetic flowmeter would be an excellent in-core instrument.

F. Hot Wire Anemometer

The hot wire anemometer has been successfully used to measure the flow rate of gases and has only recently been applied to the measurement of liquid flow rates. A hot wire anemometer is a thin wire mounted on supports, as shown in Figure III-17, through which an electric current is passed. The voltage across the wire depends on the wire resistance, which depends on its temperature, which in turn depends on the cooling effect or velocity of the flowing fluid.

---

[14] Elrod, H. J., Jr., and Fouse, R. R., An Investigation of Electromagnetic Flowmeters, Transactions of the ASME, 74, 589-594 (1952).

[15] Wichner, R. P., Slurry Flowmeters and Density Meters for Homogeneous Reactors, ORNL-CF-57-9-96.

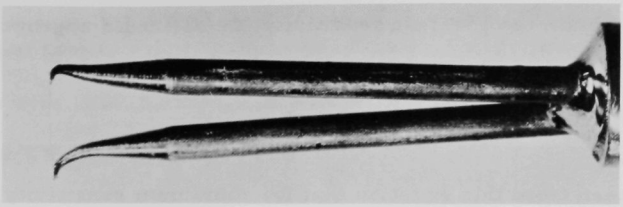

Fig. III-17

Hot Wire Anemometer

Two types of circuits are normally used with a hot wire probe. One is called a "constant current" system and the other a "constant temperature" system. With the constant-current system, the heating current is kept constant and the voltage across the hot wire is examined. The response of the hot wire to velocity fluctuations is modified by the heat capacity of the wire when a constant current is maintained. In the constant-temperature system, a feedback circuit maintains a constant wire resistance and, hence, its temperature. The input energy to this system must go entirely into the fluid and the heat capacity of the wire becomes of little importance, as its temperature is constant and the input energy is a measure of the instantaneous velocity.

The hot wire anemometer was also seriously considered for in-core use. Its small size and simple construction were particularly attractive. A design study was undertaken to determine the optimum size, material, and operating conditions of a solid wire probe which would have maximum sensitivity for a given set of system parameters. Because of its improved response time, a constant-temperature probe was investigated.

Empirically, for circular cylinders operated at constant temperature, velocity and current can be related by the following equation:

$$V = \left[\frac{I^2K_4 - K_1K_3}{K_2(K_1 - I^2)}\right]^{1.923} , \qquad \text{(III.10)}$$

where

$$K_1 = (14.82)\, D_0^2\, (\bar{K}_m/\bar{\rho}_m)(\bar{t} - t_w)$$

$$K_2 = 0.47\, K_f(\rho_f D_0/0.1\mu_f)^{0.52}\, (0.1\, C_p\mu_f/K_f)^{0.3}$$

$$K_3 = (0.35)K_f\,(0.1\, C_p\mu_f/K_f)^{0.3}$$

$$K_4 = K_2 + 6\bar{K}_m$$

To obtain the greatest sensitivity, dv/dI should approach zero. From Equation III.10,

$$\frac{dV}{dI} = \frac{3.847\ IK_1\ [K_4 - K_3][I^2K_4 - K_1K_3]^{0.923}}{1.923\,K_2(K_1 - I^2)^{2.923}} \quad . \qquad \text{(III.11)}$$

It can be seen from this equation that for maximum sensitivity, $\bar{K}_m/\bar{\rho}_m$ and $\Delta t$ must be as large as possible. The sensitivity can also be increased by using a large-diameter wire, $D_0$, and large heating current I.

A sample calculation is now presented to illustrate the use of these equations. A probe will be designed with the following system parameters given:

System Pressure - 41.8 atm

Maximum Water Temperature - 249.5°C

Maximum Water Velocity - 1.52 meters/sec

Power Available - 2 watts at 0.5 amp

Length of Probe not to Exceed 0.635 cm.

Since it is desirable to have $\Delta t$ as large as possible, $\bar{t}$ will be fixed at the saturation temperature corresponding to the pressure of the system. Now a metal must be selected that will not corrode in water, will not change resistance with time, will be strong and rigid enough to withstand the flow without breaking, and which will have a large $\bar{K}_m/\bar{\rho}_m$ ratio. Tungsten appears to be a good choice. The water temperature is 249.5°C and the saturation temperature corresponding to 41.8 atm is 252.3°C; therefore, the minimum $\Delta t$ will be 2.8°C. Now $D_0$ can be computed by fixing I = 0.5 amp and V = 1.52 m/sec. The water properties are evaluated at $t_f$, the film temperature, which is now assumed equal to $\frac{1}{2}(\bar{t} + t_w)$, and the metal properties are evaluated at $\bar{t}$. For the system and probe mentioned above $K_1$, $K_2$, $K_3$, $K_4$, I, and V are either given or can be calculated.

Substituting the values obtained in Equation (III.10), and solving for $D_0$,

$$D_0 = 0.028 \text{ mm.}$$

Knowing the diameter and length of the probe, the maximum power dissipated in the probe can now be computed.

$$\bar{R} = \rho_m\, L/A = 1.285 \text{ ohms}$$

$$P_{max} = I^2\bar{R} = (0.5)^2\,(1.285) = 0.321 \text{ watt.}$$

It had been assumed that $\frac{1}{2}(\overline{t} + t_w)$ is a good approximation to $t_f$, which is actually equal to $\frac{1}{2}(t_0 + t_w)$. This assumption can now be verified.

The wire heat flux, q", is given by

$$q'' = 6\overline{K}_m(\overline{t} - t_0)/\pi D_0$$

and also

$$q'' = I^2\overline{R}_1/\pi D_0 L \quad .$$

Equating the above equations,

$$\overline{t} - t_0 = I^2\overline{R}_1/6\overline{K}_m L$$

$$t_0 = \overline{t} - I^2\overline{R}_1/6\overline{K}_m L$$

$$t_0 = \overline{t} - 0.054°C.$$

It can be seen that the initial approximation that $\overline{t} = t_0$ was a good one and would not significantly affect the value of the water properties appearing in Equation (III.10). The main concern is to keep $t_0$ just slightly under the system saturation temperature in order to prevent local boiling.

We have now enough information to plot the velocity-current curves for the given probe. Figure III-18 shows this plot and the effect of varying $\Delta t$.

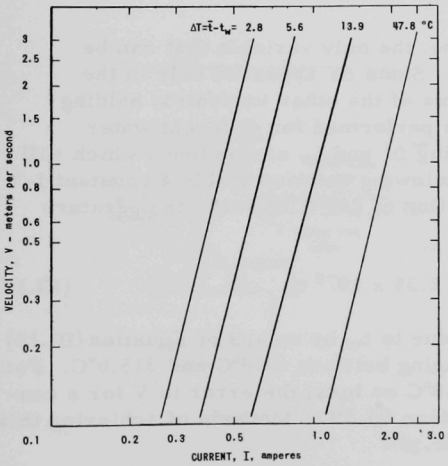


Fig. III-18

Current-Velocity Relationships for a 0.028-mm Tungsten Wire Operating at an Average Temperature of 252°C with Varying Water Temperatures

From Figure III-18, it can be seen that as $\bar{t}$ is held constant and $t_w$ varies, an undesirable family of curves results. If $\Delta t$ is held constant by some means (see Figure III-19), the spread in the family of curves improves, but still does not result in a constant I-V locus. To obtain a constant I-V locus, some sort of water temperature compensation must be used. The effects of system pressure can be neglected.

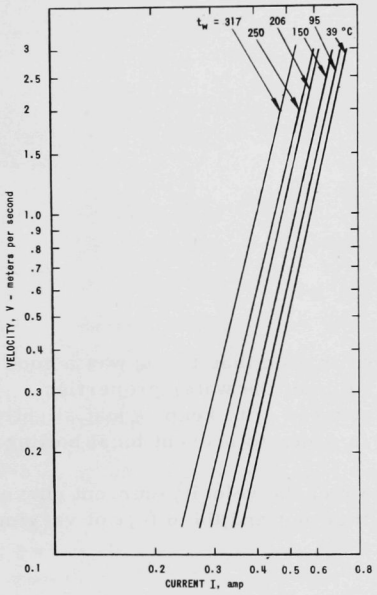


Fig. III-19

Current-Velocity Relationships for a 0.028-mm Tungsten Wire Operating with a Constant 2.8°C $\Delta t$ with Varying Water Temperature

For a given system and probe, the only variable that can be maneuvered for compensation is $\Delta t$. Since $\Delta t$ appeared only in the term $K_1$, it can be solved for in terms of the other variables, holding I and V constant. If the operation is performed for different water temperatures, a relationship involving $\Delta t$ and $t_w$ can be found which will yield a particular I-V locus. The following relation yields a constant I-V locus good to within 20T for a variation of 260°C in water temperature for this sample system and probe:

$$\Delta t = 1.87 - 2.01 \times 10^{-3} t_w + 2.35 \times 10^{-5} t_w^2 \quad . \qquad \text{(III.12)}$$

The reduction in variations due to $t_w$ by means of Equation (III.12) is shown in Figure III-20 for $t_w$ ranging between 37.8°C and 315.6°C. For water temperature variations of 37.8°C or less, the error in V for a constant I is under 5% if $t_w$ is greater than 93.3°C. Methods of achieving this compensation will be discussed later.

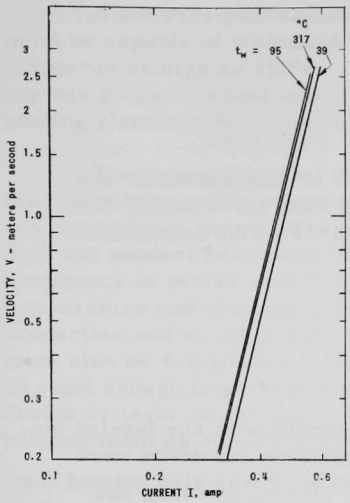


Fig. III-20

Current, Velocity Relationship for a 0.028 mm Tungsten Wire Operating with $\Delta T$ Varying as $1.87\text{-}2.01 \times 10^{-3} T_w + 2.35 \times 10^{-5} T_w^2$

To test the validity of Equation (III.10), a simple experimental loop was built. The experiment was performed at atmospheric pressure with ordinary tap water, and no attempt was made to obtain maximum probe sensitivity. The probe used was made of a platinum wire, 0.127 mm in diameter and 6.35 mm in length, mounted on a 1.016-mm-diameter manganin wire. The leads from the platinum wire were insulated from each other by using ceramic tubing, and they constituted one leg of a Wheatstone bridge. The Wheatstone bridge was wired with manganin wire wherever possible in order to keep the resistances constant over a large current range. The water temperature during the test was held constant, and therefore no temperature compensation was necessary. By measuring the current required to keep the bridge balanced and by measuring the fluid velocity with another flow meter, a current-velocity relationship was obtained. Data were taken for two different subcoolings and for velocities ranging from 0.152 to 1.52 m/sec. Diagrams of the loop and probe are shown in Figure III-21, and the data are plotted and compared with predictions of Equation (III.10) in Figure III-22.

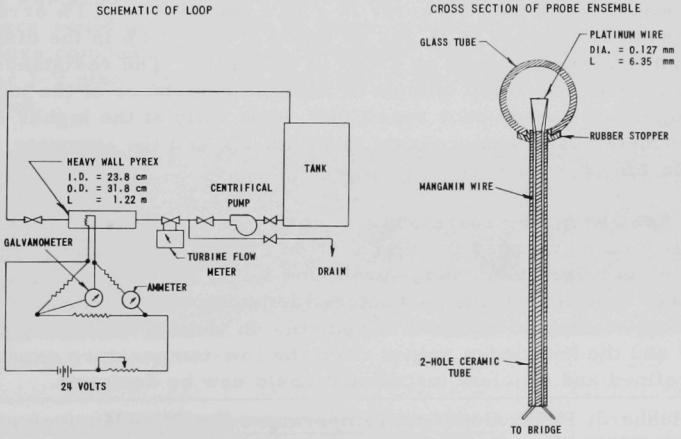


Fig. III-21

Schematic of Loop and Cross Section of Probe Ensemble

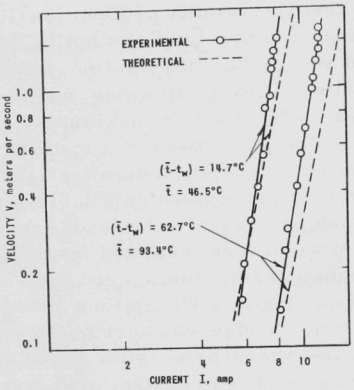


Fig. III-22

Comparison of Experimental and Theoretical Current-Velocity Relationship for Hot Wire Anemometer

It was found that the probe was very sensitive to any foreign material that formed on it. Erratic meter fluctuations and drifts were noticed, indicating a serious need for screening. It was also noticed that when a clean probe was used, there were abnormal drifts to zero on the ammeter. This difficulty was overcome by turning the power off and then on again after a short period of time. Hubbard[16] attributes this phenomena to polarization effects but offers no final solution.

When considering the discrepancy between the theoretical and experimental curves, it must be realized that the heat transfer coefficient[17] used in Equation (III.10) is only an estimate good to within 20%. Also, certain parameters markedly affect the resulting I-V relationship. As an example, for I = 0.5 amp and V = 1.52 meters/sec, a 1% error in either $t_w$ or $\bar{t}$ would result in a 2% error in V at a constant I. A 1% error in I would cause a 4% error in V, and an error of only 0.1% in the diameter of the hot wire would cause an error of 2.4% in V. The resistance of the platinum probe was small compared with the resistance of the top leg of the bridge; this caused poor sensitivity, especially at the higher currents. The flowmeter used was accurate to within 1%, and the ammeter was good to within 1%.

Even with the experimental errors mentioned above, the experiment was enlightening because it showed, from Figure III-22, that the performance of a solid hot wire anemometer probe for liquid service can be approximately predicted. The difficulties encountered demonstrated the need for more refined apparatus and methods of control. In view of the theory presented earlier and the knowledge gained from the low-temperature experiments, a more refined and efficient instrument could now be designed.

---

[16] Hubbard, P. G., Constant Temperature Hot Wire Anemometer with Applications to Measurements in Water, Ph.D. Thesis, University of Iowa (June 1954).

[17] McAdams, W. H., Heat Transmission, McGraw-Hill Book Co., Inc., New York 2nd Edition, (1942) Ch. 8, p. 222.

A hot wire probe ensemble for loop testing must be portable and must be capable of withstanding pressures as high as 81.8 atm and temperatures as high as 252°C. The problem of sealing, insulating, and mounting this probe in a test loop is not a difficult problem, as a conventional sealing gland can be converted for use with a probe.[18]

The mount material must possess a low thermal conductivity, a low resistivity, a low temperature coefficient of resistance, and must be noncorrosive in water. These properties are desirable so that the mount does not conduct heat away from the wire probe, does not contribute much resistance in series with the wire, and does not change resistance due to temperature and velocity fluctuations. Inconel possesses all of these properties and would, therefore, make a good mount material. The mounts must also be designed to minimize local turbulence near the hot wire and be rigid enough to prevent vibration in the fluid stream. These desired design criteria can be accomplished by tapering the mounts to a point, bending them up stream, and welding the hot wire to them under tension.[19]

The probe ensemble, shown in Figure III-23, was designed for a 41.8-atm system with an approximate flow range from 0.03 to 0.61 m/sec. Insulation was achieved by using ceramic tubing and Teflon which was enclosed in the stainless steel tube. The Inconel mounts were machined on a lathe to approximately 0.0763-mm-diameter points and were then bent to the desired shape. Tungsten wire, 0.0254 mm in diameter and 0.546 cm in length, was then welded under tension across the mount tips. The portion of the probe exposed to the stream was held rigid by sealing the Inconel rods to the stainless steel tube with glass.

It was known in advance that, in the system to be used for this study, there would be variations of water temperature. A method of water temperature compensation had to be devised which would maintain a particular I-V plot. There are two ways in which this compensation can be achieved.

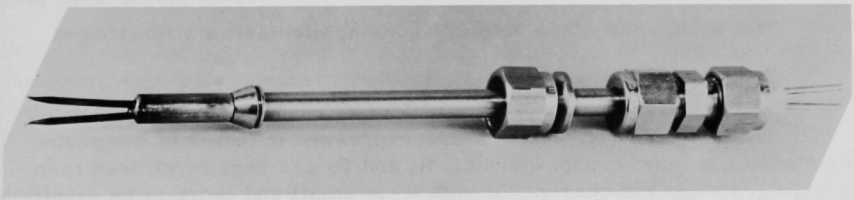

Fig. III-23

Hot Wire Anemometer Probe Assembly

[18] Conax Catalog of Thermocouple Assemblies and Pressure Sealing Glands.

[19] Lowell, Herman H., Design and Applications of Hot-Wire Anemometers for Steady State Measurements at Transonic and Supersonic Airspeeds, NACA, TN-2117.

The first way would be to insert a second leg of the original Wheatstone bridge in the water stream. By choosing a leg on the high-resistance side of the bridge, the power dissipated would be small, and the resistance of this leg would only be sensitive to actual temperature changes in the water and not to the velocity of the stream. This method of compensation can be better understood by discussing the sample Wheatstone bridge shown below.

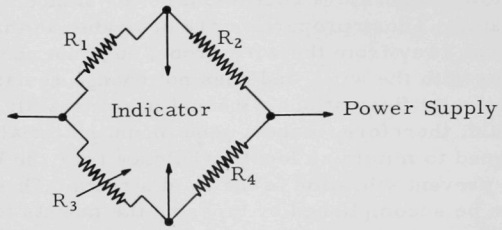


$R_1$ Velocity-sensing probe

$R_3$ Temperature-compensating leg

In discussing the sample system and probe earlier, it was found that a constant I-V plot could be obtained by expressing $\Delta t$ as a function of $t_w$. From Equation (III.12),

$$\Delta t = f(t_w) \quad .$$

Since

$$\Delta t = \bar{t} - t_w \quad ,$$

it follows that

$$\bar{t} = t_w + f(t_w) \quad .$$

The resistance of the velocity-sensing element is a function of

$$\bar{R}_1 = f(\bar{t}) = f_1(t_w) \quad .$$

The desired $\Delta t$ function is now expressed in terms of the probe resistance. In most bridge circuits, $R_1$ and $R_2$ are very much less than $R_3$ and $R_4$, so that the current through $R_3$ is small and there is no significant heating effect. Resistance $R_3$ must now be chosen so that when it is immersed in the water stream its resistance will vary with $t_w$ in such a way as to yield a bridge balance at $\bar{R}_1 = f_1(t_w)$ which corresponds to a particular I-V plot. For the bridge shown,

$$R_3 = \bar{R}_1 R_4 / R_2 \quad ,$$

where $R_4$ and $R_2$ are constant. Therefore,

$$R_3 = f_1(t_w) R_4/R_2 \quad .$$

The easiest way to achieve this compensation is to make $\bar{R}_1$ and $R_3$ out of the same material.

The second method of compensation would be to connect a relatively large-diameter wire in series with the probe, both being immersed in the water stream.[16] Because of the large diameter, the heating is slight and the resistance would only depend on the water temperature.

The first method of water compensation was tried. Approximately, 36 cm of 0.0254-mm tungsten wire was wrapped around a threaded ceramic tube which was sealed in the same way as the velocity element.

A Wheatstone bridge was used to keep the probe at a constant resistance, i.e., a constant temperature. A control system connected to the bridge error signal was used to adjust automatically the heating current through the probe. Probe current was measured by noting the voltage drop across a 1-ohm resistor which constituted a second leg of the Wheatstone bridge.

The results of this experiment were not very encouraging. No meaningful data could be obtained during the time allotted for testing. The major difficulty was the consistent breaking of the wire probe. Further investigation revealed that the stresses in the tungsten wire were high enough to cause fractures when the flow rate was as low as 0.5 m/sec if the temperature of the wire was 252°C.

The problem remaining, then, is to investigate other materials for the wire elements at high temperatures. If this problem can be solved, the hot-wire anemometer, because of its small size and fast response, may be a useful device for measuring flow rates in a nuclear reactor.

## G. Nomenclature

| | |
|---|---|
| $A$ | Wire cross-sectional area (square meters) |
| $A_1$ | Inlet flow area (square meters) |
| $A_2$ | Throat flow area (square meters) |
| $C$ | Calibration coefficient |
| $C_p$ | Specific heat of water evaluated at $t_f$ (watt-sec/kg-°C) |
| $D_0$ | Wire outside diameter (meters) |
| $g$ | Gravitational constant (meters/sec$^2$) |
| $h_f$ | Enthalpy of saturated liquid (watt-sec/kg) |
| $h_{fg}$ | Enthalpy change during vaporization (watt-sec/kg) |
| $h_g$ | Enthalpy of dry saturated vapor (watt-sec/kg) |
| $h_{in}$ | Enthalpy of inlet water (watt-sec/kg) |
| $h_{Iin}$ | Enthalpy of water into ion exchanger (watt-sec/kg) |
| $h_{Iout}$ | Enthalpy of water out of ion exchanger (watt-sec/kg) |
| $h_m$ | Enthalpy of mixed feedwater (watt-sec/kg) |
| $h_m$ | Enthalpy of feedwater (watt-sec/kg) |
| $I$ | Current (amp) |
| $K$ | Calibration coefficient |
| $K_f$ | Thermal conductivity of water evaluated at $t_f$ (watts/meter-°C) |
| $\overline{K}_m$ | Thermal conductivity of wire material evaluated at $\overline{t}$ (watts/meter-°C) |
| $L$ | Wire length (meters) |
| $n$ | Area ratio $A_1/A_2$ |
| $P_{max}$ | Maximum power dissipated in wire (watts) |
| $q''$ | Heat flux (watts/square meter) |
| $Q_t$ | Total power generated (watts) |
| $\overline{R}_1$ | Wire resistance evaluated at $\overline{t}$ (ohms) |
| $\overline{t}$ | Average temperature of wire $\left(\frac{2t_1 - t_0}{3}\right)$ (°C) |
| $t_f$ | Film temperature $\left(\frac{t_w + t_0}{2}\right)$ (°C) |
| $t_w$ | Water temperature (°C) |

| | |
|---|---|
| $t_1$ | Center line temperature of wire (°C) |
| $t_0$ | Surface temperature of wire (°C) |
| V | Water velocity (meters/sec) |
| $W_I$ | Ion exchange flow rate (kg/sec) |
| $W_m$ | Feedwater flow rate (kg/sec) |
| $W_s$ | Total steam flow rate (kg/sec) |
| $W_{s1}$ | Steam discharge flow rate (kg/sec) |
| $W_{s2}$ | Entrained steam flow rate (kg/sec) |
| $W_t$ | Total recirculation flow rate (kg/sec) |
| $x_D$ | Steam entrainment in the downcomer |
| $x_e$ | Average core exit quality |
| $\Delta P$ | Differential pressure (atm) |
| $\Delta t$ | $\overline{t} - t_w$ (°C) |
| $\mu_f$ | Water absolute viscosity evaluated at $t_f$ (poise) |
| $\rho$ | Water density (kg/cubic meter) |
| $\rho_f$ | Water density evaluated at $t_f$ (kg/cubic meter) |
| $\overline{\rho}_m$ | Wire resistivity evaluated at $\overline{t}$ (ohm-meter) |

# IV. MODERATOR STEAM VOID FRACTION

## A. Introduction

The steam void fraction is defined as the volume percentage of steam present in a unit volume of coolant. The steam void fraction is actually more important than the inlet velocity when predicting the static and dynamic behavior of the boiling water type of reactor. As there were no commercial instruments available to measure this parameter in the core, suitable techniques and instruments had to be developed.

## B. Turbine-type Flowmeters

For a system, as shown in Figure IV-1, where liquid enters at the bottom of a fuel element and a two-phase mixture leaves the top, the two-phase continuity equations can be written as follows.

$$(1 - x_e)\, W_t = W_{fe} = \rho_f (1 - \bar{\alpha}_c)\, A_e\, V_{fe} \qquad \text{(IV.1)}$$

and

$$W_t = \rho_{in}\, A_{in}\, V_{in}. \qquad \text{(IV.2)}$$

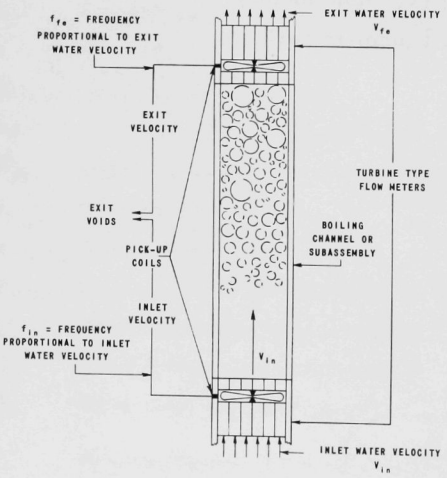


Fig. IV-1

Schematic of Turbine Flowmeters Applied to a Boiling System

Upon combination of Equations (III.1) and (III.2), the void fraction is obtained as

$$\bar{\alpha}_c = \frac{\rho_f A_e V_{fe} - \rho_{in} A_{in} V_{in} (1 - x_e)}{\rho_f A_e V_{fe}} \quad ; \qquad \text{(IV.3)}$$

which can be simplified as follows. The flow areas $A_e$ and $A_{in}$ can be made equal by employing two identical meters. Now, if we neglect the effects of subcooling and quality, the void fraction is equal to

$$\overline{\alpha}_c = 1 - \frac{V_{in}}{V_{fe}} \quad . \tag{IV.4}$$

With equal flow areas, Equation (IV.3) can be rearranged as follows:

$$\overline{\alpha}_c = 1 - \frac{\rho_{in}(1 - x_e)\, V_{in}}{\rho_f\, V_{fe}} \quad . \tag{IV.5}$$

The subcooling and quality effects can be neglected in some boiling systems because they are small. In other systems, they can be neglected because, as the quality $x_e$ increases, $(1 - x_e)$ decreases. As quality increases, the subcooling should also increase if it may be assumed that there is no steam carry-under into the down-comer; hence the ratio $\rho_{in}/\rho_f$ also increases. Therefore, the product of $(1 - x_e)$ and $\rho_{in}/\rho_f$ in Equation (IV.5) remains very close to unity. At a typical loop operating condition, for example, the exit mixture quality, $x_e$, is 0.08 and the subcooling is 18.3°C. With these values of quality and subcooling, the error in computing void fraction by means of Equation (IV.4) is only about 4%.

This means that if only the inlet and outlet liquid velocities are known, the void fraction can be determined with a fair accuracy. However, the inlet subcooling is measured and, from Equation (III.5), the average exit quality is calculated, and hence the exit void fraction can be calculated more exactly.

It appeared that a turbine-type flowmeter might measure this exit liquid velocity, so an analysis was made of the turbine response when a two-phase mixture was passed by it. This analysis was based on an adaptation of Grey's analysis[20] for the transient response of a turbine flowmeter.

For a turbine rotating in incompressible, nonviscous fluids with negligible bearing friction, the rotor torque can be written as

$$T = I \frac{d\theta^2}{d\tau^2} \quad , \tag{IV.6}$$

---

[20] Grey, J. Transient Response of the Turbine Flowmeter, Jet Propulsion (Feb 1956).

where T is rotor torque, I the moment of inertia of rotor, and $\frac{d\theta^2}{d\tau^2}$ is angular acceleration. Now from Figure IV-2,

$$dT = Frdr \quad . \tag{IV.7}$$

For steady state, however,

$$dT = 0$$

and

$$F = 0 \quad .$$

Now

$$F = -F'_f \cos \delta_f + F'_g \cos \delta_g = 0, \tag{IV.8}$$

where F' is the force per unit blade length perpendicular to effective velocity U.

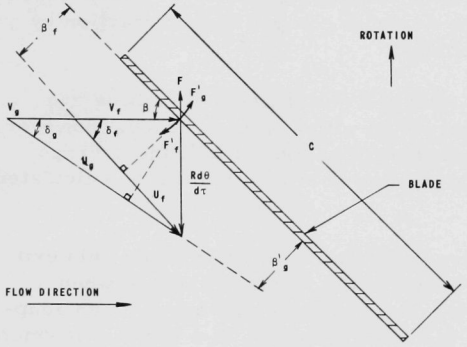


Fig. IV-2

Hydrodynamic Forces on a Blade Subjected to a Two-phase Mixture

By definition,

$$C_L' = \text{lift coefficient} \equiv 2F'/C\rho U^2 \tag{IV.9}$$

$$C_L = \frac{2F' \cos^2 \delta}{C \rho V^2}$$

$$C_g = \bar{\alpha}_c C$$

$$C_f = (1 - \bar{\alpha}_c) C \quad .$$

For a blade of finite length, the effect of induced drag must be introduced and

$$C_L' = K \sin \beta' \quad . \tag{IV.10}$$

Therefore, from Equation (IV.8)

$$- \frac{\sin \beta_f' \rho_f V_f^2 (1 - \bar{\alpha}_c)}{\cos \delta_f} + \frac{\sin \beta_g' \rho_g V_g^2 \bar{\alpha}_c}{\cos \delta_g} = 0 \quad , \tag{IV.11}$$

where

$\beta'$ is effective angle of attack = $\beta - \delta$

$\delta$ is $\tan^{-1} \left( \frac{R \, d\theta}{d\tau} \Big/ V \right)$

$\rho$ is fluid density

$\beta$ is blade angle with pipe axis

V is flow velocity

R is mean radius

$\frac{d\theta}{d\tau} = \omega$ = rotor speed,

and subscripts f refers to water and g to gas. Now

$$\frac{\sin(\beta - \delta_f) \rho_f V_f^2 (1 - \bar{\alpha}_c)}{\cos \delta_f} = - \frac{\sin (\beta - \delta_g) \rho_g V_g^2 \bar{\alpha}_c}{\cos \delta_g} \quad . \tag{IV.12}$$

Accordingly

$$\frac{d\theta}{d\tau} = \omega = \frac{\tan \beta}{R} \left[ \frac{\rho_f V_f^2 (1 - \bar{\alpha}_c)}{\rho_g V_g \bar{\alpha}_c} + \frac{\rho_g V_g^2 \bar{\alpha}_c}{\rho_f V_f (1 - \bar{\alpha}_c)} \right] \tag{IV.13}$$

where $\frac{\tan \beta}{R}$ is a meter constant.

Now by definition,

$V_g / V_f$ = S = slip ratio.

Therefore,

$$\omega = \frac{\tan\beta}{R} V_f \left[\frac{(1 - \overline{\alpha}_c)\ \rho_f + \overline{\alpha}_c\ \rho_g\ S^2}{(1 - \overline{\alpha}_c)\ \rho_f + \overline{\alpha}_c\ \rho_g\ S}\right] . \qquad \text{(IV.14)}$$

The error in measuring the local liquid velocity is the term

$$\left[\frac{(1 - \overline{\alpha}_c)\ \rho_f + \overline{\alpha}_c\ \rho_g\ S^2}{(1 - \overline{\alpha}_c)\ \rho_f + \overline{\alpha}_c\ \rho_g\ S}\right] .$$

If $\rho_g << \rho_f$, the error is small. If S approaches unity, the error is small.

To use the turbine meter for measuring local liquid velocity, a knowledge of the slip ratio is necessary or the gas density must be much less than the liquid density. For a 41.8-atm system, $\rho_g \approx 0.028\ \rho_f$, and if the slip is less than 2 and the void fraction of less than 0.5, the error is a maximum of 5%.

It can be seen from this analysis that the turbine will respond very closely to the water velocity even when the flowing medium is composed of a mixture of air and water or steam and water. This important discovery led to a new use for this type of meter: the measurement of exit steam void fraction within the reactor core.

To show that turbine-type flowmeters could be used successfully to measure the exit void fraction, an experimental out-of-pile flow system was built. This flow system is shown schematically in Figure IV-3.

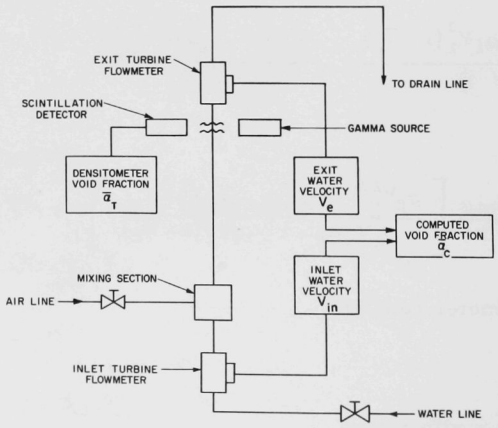


Fig. IV-3

Schematic of Air-Water Flow System

One turbine-type flowmeter was placed in a water line just after a valve that was used to regulate the inlet water velocity. A mixing section, which blended air into the flowing water, was then inserted into the system. A second flowmeter was placed several feet upstream of the mixing section. Great care was exercised to prevent expansions or contractions in flow area in this section of the piping. Expansions or contractions in flow area will disturb the two-phase mixture and will alter the void fraction. The air-water mixture was then discharged to a drain. A gamma-ray densitometer was placed just below the upper flowmeter to measure the actual void fraction. This technique for measuring void fraction is based upon the principle that, as gamma rays pass through matter, the photons are absorbed and the intensity decreases exponentially with the distance traversed. In present practice, gamma rays emanating from a radioactive source are beamed through and attenuated by the air-water mixture contained in the test channel. The attenuated radiation then impinges on a scintillation crystal which is mounted on the face of a photomultiplier tube. The crystal-tube assembly is enclosed to prevent the entrance of extraneous light. The current output of the photomultiplier tube is amplified and recorded on a strip chart recorder. The all-water and all-air radiation intensities are used as calibration points for void fractions of zero and unity, respectively. As the radiation intensity is exponentially attenuated between these two points, intermediate values of void fraction can be determined. A more detailed description of this densitometer can be found in the literature.[21]

The flow system was run to obtain void fractions ranging from 0.11 to 0.71. The range of inlet water velocity was varied from 0.61 to 2.13 m/sec. The void fraction was measured with the densitometer and simultaneously calculated from the two flow measurements by means of Equation (IV.4). The use of Equation (IV.4) is justified because the subcooling was zero and the quality was less than 0.01.

The densitometer is considered the standard for these measurements. Figure IV-4 shows the error plot of the void fractions obtained. Here $\bar{\alpha}_T$ is the void fraction determined by the densitometer and $\bar{\alpha}_C$ is the void fraction calculated from the two flow measurements. The dashed lines indicate an error of ±10%. It is apparent from this figure that the void fractions compared, in most cases, to within this ±10%. These results were encouraging enough to proceed with similar tests where the temperature and pressure conditions would duplicate those of the reactor: 252°C and 41.8 atm.

An existing natural-circulation flow "loop" was utilized for these steam-water tests. This "loop" is normally used to obtain information about natural circulation. The system, slightly modified to include the two flowmeters, is shown schematically in Figure IV-5.

---

[21] Hooker, H. H., and Popper, G. F., A Gamma-ray Attenuation Method for Void Fraction Determinations in Experimental Boiling Heat Transfer Test Facilities, ANL-5766 (1958).

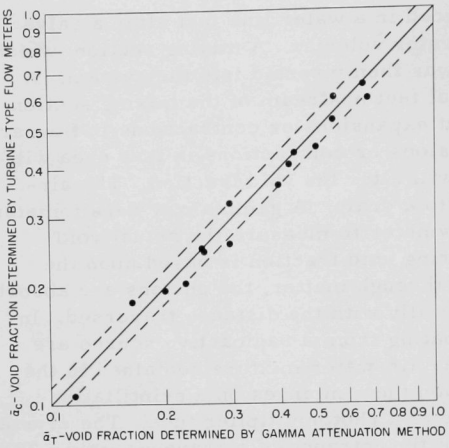


Fig. IV-4

Error Plot of Void Fractions from Air-Water Tests

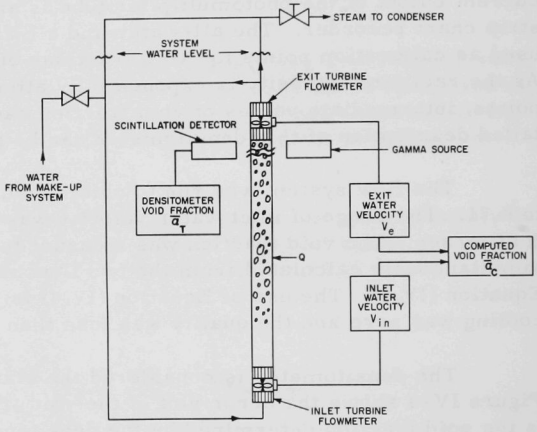


Fig. IV-5

Schematic of Natural Circulation Flow System

It consists basically of the natural-circulation system, a makeup water system, and a steam condenser. Power is applied to the resistance-heated test channel, and boiling begins. The two-phase mixture passes through the upper turbine flowmeter, up through the riser to the steam drum where the steam is separated from the water. The water then flows down through the downcomer, up through the lower turbine-type flowmeter, and back into the test channel. The gamma-ray densitometer used in the air-water test was placed just below the upper flowmeter to determine again the steam void fractions. The steam was withdrawn from the steam drum, condensed, and pumped back to the makeup system. Makeup water is added to the system to keep the water level at equilibrium.

The need for an instrument capable of displaying the void fraction directly became apparent while running the air-water tests. An electro-mechanical computer that would calculate the void fraction from Equation (IV.4) was designed and built before the steam-water tests were run. A bridge technique was used for the computer because this is a simple and accurate way of obtaining an output that is proportional to one input divided by a second input. This bridge method, however, has the disadvantage that some means of balancing, such as a servo, is required. This could seriously limit the frequency response of the computer. The computer was found to have an accuracy of ±1% and digitally displayed void fraction reliably. Because of its rather poor dynamic characteristics, it will be used only when obtaining steady-state void information.

A series of tests were run with this "loop" to obtain void fractions ranging from 0.24 to 0.70. The error plot of the void fractions obtained is shown in Figure IV-6. Here again $\overline{\alpha}_T$ is the void fraction obtained from the densitometer and $\overline{\alpha}_C$ is the void fraction calculated from the two velocity measurements; however, in this case, the computer performed the calculation. Again, the void fractions compared to within ±10% in most cases.

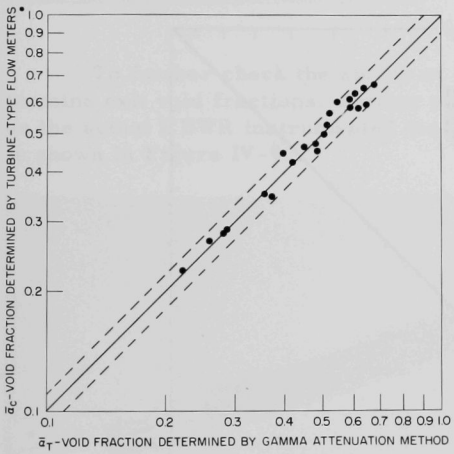


Fig. IV-6

Error Plot of Void Fractions from Steam-Water Tests

There are several limitations that must be pointed out when one uses these flowmeters to measure exit steam void fraction. First, the system in which they are used must not exceed 41.8 atm. This limitation may be removed if tests now in progress show that the meters can be used to measure void fractions in systems of higher pressure. Second, contractions or expansions in flow area between the exit of the assembly and the exit flowmeter must be minimized to prevent void fraction changes. And last, the flowmeters will introduce a pressure drop which depends upon meter size, flow rate, and void fraction.

The two-phase pressure drop across a turbine flowmeter can be predicted by the use of a very simple flow model. In this flow model, it is assumed that the air or steam phase contributes nothing to the pressure drop. The increased pressure drop is solely produced by the increased water velocity through the meter. Making this assumption, it can be shown, by combining Equation (IV.4) with the equation of the curve shown in Figure III-9, that the two-phase pressure drop is equal to

$$\Delta P_{TWP} = \frac{\Delta P_{SP}}{(1 - \bar{\alpha}_c)^2} \qquad \text{(IV.15)}$$

where $\Delta P_{SP}$ is the pressure drop across the meter when the void fraction is zero and $\bar{\alpha}_c$ is the void fraction at the flowmeter.

Figure IV-7 shows the close correspondence between the predicted and measured pressure drops. As these data represent the results from only one particular turbine flowmeter, no general statement can be made as to the validity of Equation (IV.15) to predict the two-phase pressure drops across meters of different sizes or configurations.

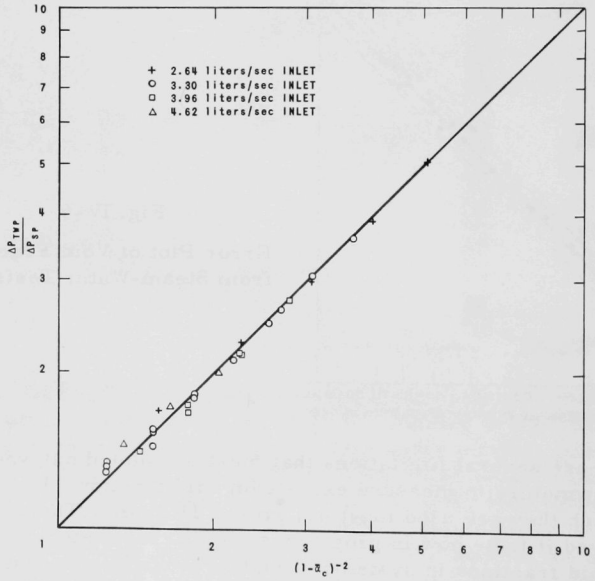


Fig. IV-7

The Ratio of Two-Phase to Single-Phase Pressure Drop for a Potter Aeronautical Model $2\frac{1}{2}$-760 Turbine Flowmeter.

The exit flowmeter that is being used in the EBWR is shown in Figure IV-8. This flowmeter is attached to the top of a standard fuel assembly in place of the normal top piece. The normal top piece is fastened on top of the flowmeter so that this subassembly can be handled with standard fuel-handling tools.

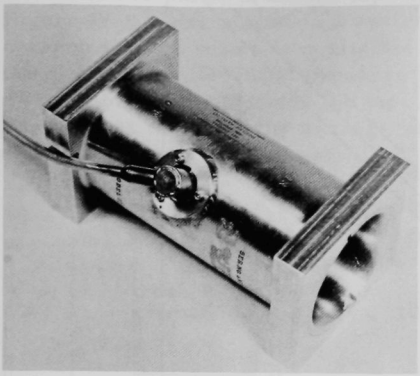

Fig. IV-8

Outlet Turbine Flowmeter

To further check the ability of the turbine-type flowmeters to determine exit void fractions, another series of out-of-pile tests were run on the actual EBWR instrumented fuel assemblies. One of these assemblies is shown in Figure IV-9.

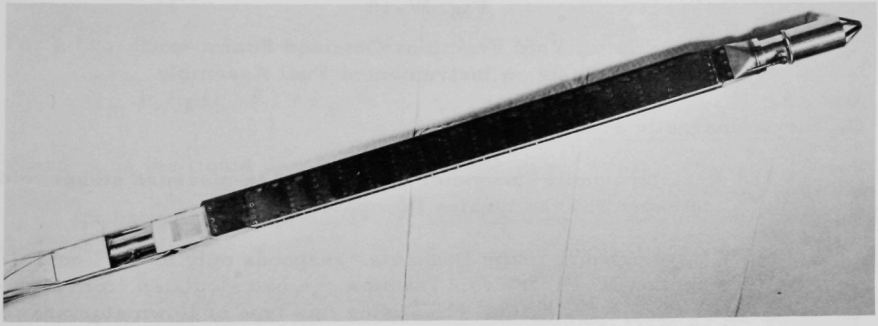

Fig. IV-9

Instrumented Fuel Assembly

This fuel element was placed in an air-water loop. The system was run to obtain void fractions ranging from 0.10 to 0.40 and inlet velocities from 0.76 to 1.22 m/sec. The void fraction at the exit of the fuel channels was again measured by means of the gamma-ray densitometer. The error

plot of the void fractions obtained by the two methods is shown in Figure IV-10. Again the voids compared to within ±10%.

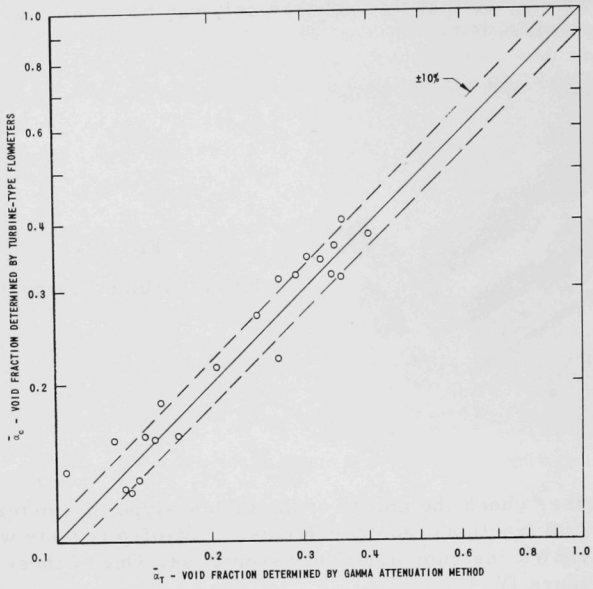


Fig. IV-10

Error Plot of Void Fractions Obtained From Air-Water Tests on Instrumented Fuel Assembly

C. Electromagnetic Flowmeters

The electromagnetic flowmeter can be used to measure steam void fractions in the same way the turbine flowmeter is used.

Since the electromagnetic flowmeter responds only to the liquid velocity (see Section III-E), the void fraction can be calculated from Equation IV.3. The advantages gained when using this type of flowmeter are that there is a low pressure drop across the meter and no correction is needed to account for the momentum of the gas phase.

One of the questionable aspects of using the electromagnetic flowmeter in this application is whether the electrodes will be covered with liquid at all times. If the electrodes become insulated from the liquid, say by steam or air pocket, the induced voltage will not be commutated and the output signal will drop to zero. This effect is presently being

investigated in an air-water loop, but no conclusive results are available at this time.

D. Pressure-drop Techniques

If two static pressure taps spaced by a distance L, as shown in Figure IV-11, are placed in a system in which the frictional pressure drop between the two points is negligible compared with the head pressure, then the measured differential pressure between the taps can be related to the mean fluid density between the taps. Also, if the fluid between the taps is a two-phase mixture, the average void fraction $\bar{\alpha}$ between the taps can be determined.

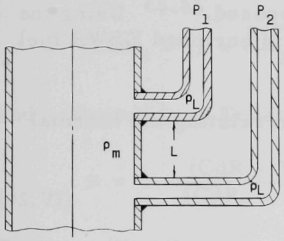


Fig. IV-11
Static Pressure Taps

For the system shown in Figure IV-11, the differential pressure between the taps is given by

$$10{,}332\ \Delta P = P_1 - P_2 = (\rho_L - \rho_m) L \quad , \tag{IV.16}$$

where $\rho_L$ is the fluid density of leg $P_2$ and $\rho_m$ is the mean fluid density of system. If $\Delta P$ is measured, and $\rho_L$ and L are known, then the fluid density is given by

$$\rho_m = \frac{\rho_L\ L - 10{,}332\ \Delta P}{L} \quad . \tag{IV.17}$$

For a two-phase mixture, however,

$$\rho_m = \rho_f (1 - \bar{\alpha}) + \rho_g\ \bar{\alpha} \quad , \tag{IV.18}$$

where $\rho_f$ is the liquid density and $\rho_g$ is the vapor or gas density.

Substituting Equation (IV.18) into Equation (IV.17) and solving for $\bar{\alpha}$,

$$\bar{\alpha} = \frac{10{,}332\ \Delta P + (\rho_f - \rho_L)\ L}{(\rho_f - \rho_g)\ L} \quad . \tag{IV.19}$$

It was also assumed in this derivation that the void fraction $\alpha$ remains constant between the taps and that temperature gradients between pressure tubes are nonexistent.

These assumptions are valid in the case of the EBWR riser and downcomer and, therefore, static pressure taps are being used for

determinations of void fraction. The problem of bringing the pressure tap tubes up through the steam zone was solved in the same manner as for the Pitot and Stauscheibe tubes mentioned earlier. The density $\rho_L$ of the fluid in the pressure top $P_2$ is determined by a temperature measurement.

Out-of-pile tests were conducted to determine void fractions with pressure taps of the type installed in EBWR. The void fraction was determined by this pressure-drop method and compared with the void fractions determined by the gamma-ray densitometer. No significant deviations between the two measured void fractions were found.

E. Nuclear Void Meters

Several nuclear void meters have been proposed.[22,23] Using the method proposed by Untermeyer, the voids in a thin enriched EBWR fuel element were measured by Thie and Beidelman.[23]

In multigroup diffusion theory, the equation relating the thermal flux $\phi_3$ and the epithermal flux $\phi_2$ is:

$$-\nabla D_3 \nabla\phi_3 + \Sigma_{a3} \phi_3 = \Sigma_{R2} \phi_2 \quad . \tag{IV.20}$$

In typical light water power reactors, the first term is small and the thermal to epithermal flux ratio is the ratio of removal to absorption cross sections corrected for thermal leakage:

$$\frac{\phi_3}{\phi_2} = \frac{\Sigma_{R2}}{\Sigma_{a3}(1 + L^2B^2)} = K(Z,\alpha)\,(1 - \alpha) \quad . \tag{IV.21}$$

This equation introduces the almost constant $K(Z,\alpha)$, by taking advantage of the fact that $\Sigma_{R2}$ is very nearly proportional to $(1 - \alpha)$. Other effects contributing a slight dependence of K upon Z came from $\alpha$, $\Sigma_{a3}$, $L^2$, and $B^2$.

The cadmium ratio of a material having a thermal cross section $\sigma_{a3}$ (0.0253 ev) and an epithermal cross section,

$$\sigma_{a2} = \int_{E_c}^{E_0} \sigma_a \frac{dE}{E} \Bigg/ \int_{E_c}^{E_0} \frac{dE}{E} \tag{IV.22}$$

is given by

---

[22] Ager-Hanssen, H., and Dφderlein, J. M. A Method for Measuring Steam Voids in Boiling Water Reactors, Proc. 2nd UN Intern. Conf. Peaceful Uses Atomic Energy, Geneva, Switzerland, 11, 465 (1958).

[23] Material taken from EBWR Test Reports, ANL-6229 (1960), pp. 284-289. Original work of J. A. Thie and J. Beidelman.

$$CdR = \frac{\phi_2 \sigma_{a2} + \phi_3 \sigma_{a3} (0.0253) A(Z,\alpha)}{\phi_2 \sigma_{a2}} = 1 + \frac{\phi_3}{\phi_2} \frac{\sigma_{a3}}{\sigma_{a2}} (0.0253)\ A(Z,\alpha) \quad , \tag{IV.23}$$

where $A(Z,\alpha)$ is a factor which takes the shape of the local thermal spectrum into account. Substitution of Equation (IV.23) into Equation (IV.21) makes it possible to determine $\alpha$ from the measured cadmium ratio:

$$\alpha = 1 - \frac{(CdR - 1)\ \sigma_{a2}}{K(Z,\alpha)\ \sigma_{a3}\ (0.0253)\ A(Z,\alpha)} \quad . \tag{IV.24}$$

If $\alpha = \alpha_0$ at $Z_0$, then

$$(CdR_0 - 1) = \frac{K(Z_0, \alpha)\ A\ (Z_0, \alpha)\ \sigma_{a3} (0.0253)\ (1 - \alpha_0)}{\sigma_{a2}} \quad , \tag{IV.25}$$

and substitution of Equation (IV.25) into Equation (IV.24) gives

$$\alpha = 1 - \frac{(CdR - 1)}{(CdR_0 - 1)} (1 - \alpha_0) \frac{K(Z_0, \alpha)\ A\ (Z_0, \alpha)}{K(Z,\alpha)\ A\ (Z,\alpha)} \quad . \tag{IV.26}$$

Equation (IV.26) can be approximated as

$$\alpha = 1 - \frac{(CdR - 1)\ (1 - \alpha_0)}{CdR_0 - 1} \quad . \tag{IV.27}$$

The term:

$$\frac{K(Z_0,\alpha)\ A(Z_0,\alpha)}{K(Z,\alpha)\ A(Z,\alpha)}$$

can be determined by evaluating the cadmium ratios according to Equation (IV.23) by using the fluxes obtained from rigorous three-group, multiregion calculations. Since the voids are not experimentally known, at least two cases having different values of average void fraction must be assumed. The experimental cadmium ratios are then used in combination with the calculated correction term to determine the void fraction. It should be pointed out that no "vicious circle" exists, for the assumption of a particular void distribution in computing the correction is only for the purpose of refining the method.

Bare- and cadmium-covered cobalt wires were irradiated in the core of EBWR. The reactor was run at a steady power of 42.7 Mw for 5.88 hr. The wires were then counted in 1-in. increments by an automatic counting system. Since the boiling boundary was estimated at Z = 29.5 cm, $Z_0$ was chosen as 21.8 cm in order to be sufficiently far away from the bottom reflector and boiling boundary. Some nucleate bubbles were present at this point, and this effect was taken into account by assuming $\alpha_0 = 0.044$.

The cadmium ratios were then used in combination with correction factors calculated for a value of 0.2125 for $\bar{\alpha}$ as it was found to be more consistent with the void fractions determined.

Figure IV-12 shows the void fractions obtained from the experiment compared to the void fractions predicted from performance calculations.

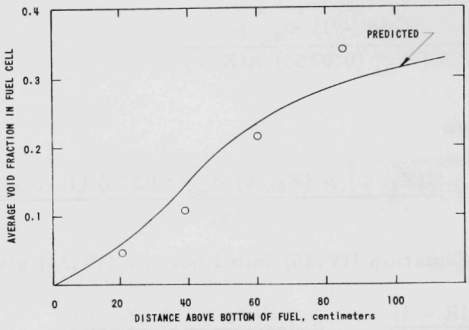


Fig. IV-12

Void Fractions Obtained From Measured Cadmium Ratio Compared to Predicted Void Fraction

There are plans to repeat this experiment using miniature in-core flux monitors in place of the cobalt wires. Only one point along the element length will be investigated, however. The advantage of using chambers is that the void fraction can be studied at many reactor operating conditions, both static and dynamic. A bare- and cadmium-covered chamber will be placed in a diagonally opposite corner of a fuel assembly and in the same axial plane. From the measured cadmium ratio, the void fraction at this point will be calculated by means of the same procedure as for the wires.

## F. Nomenclature

| | |
|---|---|
| A | Constant |
| $A_e$ | Total exit flow area (square meters) |
| $A_{in}$ | Total inlet flow area (square meters) |
| $B^2$ | Buckling (1/square meters) |
| C | Chord length (meters) |
| $C_L'$ | Lift coefficient |
| CdR | Cadmium ratio at position Z |

| | |
|---|---|
| $CdR_0$ | Cadmium ratio at position $Z_0$ |
| $D_3$ | Diffusion coefficient (meters) |
| E | Neutron energy (ev) |
| F | Force (Newtons) |
| F' | Force per unit blade length (Newtons/meter) |
| I | Moment of inertia of turbine rotor (kg-square meter) |
| K | Constant |
| L | Spacing between pressure taps (meters) |
| $L^2$ | Diffusion length (square meters) |
| $P_1$ | Pressure at tap 1 (atm) |
| $P_2$ | Pressure at tap 2 (atm) |
| r | Turbine blade radius (meters) |
| R | Mean turbine blade radius (meters) |
| S | Slip ratio - $V_g/V_f$ |
| T | Turbine rotor torque (Newton-meters) |
| U | Effective velocity (meters/sec) |
| V | Velocity (meters/sec) |
| $V_{fe}$ | Liquid exit velocity (meters/sec) |
| $V_{in}$ | Liquid inlet velocity (meters/sec) |
| $W_{fe}$ | Liquid recirculation flow rate (kg/sec) |
| $W_t$ | Total recirculation flow rate (kg/sec) |
| $X_e$ | Exit quality |
| Z | Axial fuel element position (meters) |
| $Z_0$ | Axial fuel element position for small void fraction (meters) |
| $\alpha$ | Steam void fraction at any position Z |
| $\alpha_0$ | Steam void fraction at position $Z_0$ |
| $\overline{\alpha}$ | Average steam void fraction |
| $\overline{\alpha}_c$ | Calculated exit steam void fraction |
| $\overline{\alpha}_T$ | True steam void fraction |
| $\beta$ | Turbine blade angle with pipe axis (radians) |
| $\beta'$ | Effective angle of attack = $\beta - \delta$ (radians) |

| | |
|---|---|
| $\delta$ | $\tan^{-1} \frac{Rd\theta}{d\tau} / V$ |
| $\theta$ | Angular rotation (radians) |
| $\rho$ | Density (kg/cubic meter) |
| $\rho_f$ | Saturated liquid density (kg/cubic meter) |
| $\rho_g$ | Dry saturated vapor density (kg/cubic meter) |
| $\rho_{in}$ | Inlet liquid density (kg/cubic meter) |
| $\rho_L$ | Liquid density of leg 2 (kg/cubic meter) |
| $\rho_m$ | Mean mixture density (kg/cubic meter) |
| $\sigma_a$ | Microscopic crossection (b) |
| $\sigma_{a2}$ | Epithermal microscopic crossection (b) |
| $\sigma_{a3}$ | Thermal microscopic crossection (b) |
| $\Sigma_{R2}$ | Epithermal macroscopic crossection (1/meters) |
| $\Sigma_{a3}$ | Thermal macroscopic crossection (1/meters) |
| $\tau$ | Time (sec.) |
| $\phi_2$ | Epithermal neutron flux (neutrons/$cm^2$-sec) |
| $\phi_3$ | Thermal neutron flux (neutrons/$cm^2$-sec) |
| $\omega$ | Angular velocity (radians/sec) |
| $\Delta P$ | Differential pressure = $P_1 - P_2$ (atm) |
| $\Delta P_{TWP}$ | Two-phase pressure drop (atm) |
| $\Delta P_{SP}$ | Pressure drop at zero void fraction (atm) |
| $\nabla$ | Laplacian operator |

Subscripts

| | |
|---|---|
| f | liquid |
| g | vapor |

# V. STEAM ENTRAINMENT IN THE DOWNCOMER

Steam entrainment in the downcomer, which is defined in Section III-A, adversely affects the performance of a boiling system by decreasing the net driving head available and by decreasing the subcooling. It is, therefore, important that this parameter be investigated and measured.

In Section III-A, a heat balance method was used to determine the recirculation water flow rate, assuming zero steam entrainment existed in the system. If this recirculation water flow rate is measured directly, as with a Stauscheibe tube or Venturi meter, then Equation (III.3) can be used to calculate the steam entrainment. Rearranging Equation (III.3), the steam entrainment is equal to

$$X_D = \frac{(W_m + W_I)(h_f - h_m)}{W_{tM}\, h_{fg}} - \frac{(h_f - h_{in})}{h_{fg}} \quad , \qquad (V.1)$$

where $W_{tM}$ is the recirculation water flow rate measured by the Stauscheibe tube.

The average exit quality $X_{eM}$ of the reactor can be then determined from Equation (III.5) by substituting $W_{tM}$ for $W_t$ and adding $X_D$ or

$$X_{eM} = \frac{W_m}{W_{tM}} + X_D \quad . \qquad (V.2)$$

The percent steam entrained is then equal to

$$\% \text{ steam entrainment} = X_D / X_{eM} \quad . \qquad (V.3)$$

The steam entrainment in the downcomer of EBWR is presently being measured by this method.

# VI. STEAM-WATER INTERFACE LEVEL

## A. Introduction

The steam-water level of a boiling water reactor must be accurately known if methods are to be used to prevent substantial amounts of water from being carried over into the steam-discharge line. Usually the water level of the reactor is measured across a water column which does not take into account the voids inside the vessel and, therefore, represents only an equivalent water height. This equivalent water height is also usually maintained constant by means of a level controller. If the power of the reactor is increased, for instance, the voids in the vessel will increase, and if this equivalent water height is maintained constant, the actual interface level could increase to a point where it was above the steam-discharge line and substantial amounts of water would be carried over.

Several techniques that will measure the true interface level will now be presented, and in most cases the probes will be discussed as if a single instrument was being used. A single instrument could be used only if it could be moved up and down inside the vessel to seek out the position of this interface level. As movable probes are difficult to realize, several probes are usually connected at predetermined intervals, and the interface level is inferred from the measurements made at several adjacent points along the vessel height. If, for example, four ultrasonic probes, spaced at 6-cm intervals, are being used, and the first three transducers indicate a wet condition and the fourth a dry condition, then the interface level lies between the third and fourth probe. If greater accuracy is needed, more probes spaced at closer intervals would have to be used.

## B. Ultrasonic Transducers[24]

The Acoustica ultrasonic liquid level transducer is an instrument to detect very accurately the presence or absence of liquid at a point. The system consists of two components, a probe and a control unit.

The probe is a small, metal-housed transducer which is mounted inside of a tank or chamber in which the liquid is to be detected. The probe is approximately 2.54 cm in diameter and 5.08 cm in length, and is mounted with its liquid-sensing face parallel to the liquid surface at the desired monitoring level.

---

[24] Taken from Final Report on the Development of a High Temperature, High Pressure Ultrasonic Liquid Level Sensor, DO 5428, Acoustica Associates, Inc., 10400 Aviation Blvd., Los Angeles, California.

The control unit comprises a two-transistor electronic circuit for exciting the transducer and monitoring the output. It is mounted external to the tank at any convenient point. A pair of electrical leads connects the probe to the control unit.

The probe contains an ultrasonic transducer of the magnetostrictive type, which is driven by the oscillator circuit in the control unit. This excitation causes the sensitive face of the probe, which is coupled to the transducer, to be vibrated. If the face of the probe is in contact with a liquid, the acoustic loading or damping action will cause a change in the electrical impedance of the transducer. The oscillator circuit in the control unit is designed to detect this impedance change and operates a relay when the change occurs.

Sensors of this type have a number of advantages over other liquid-level sensors. First, there are no moving parts which can jam or wear out. Second, the system is accurate to about ±0.4 mm limited only by the meniscus effect of the liquid. Third, the device is not affected by foam, vapor, or pressure. And fourth, the sensor is small and rugged.

In developing this sensor, the major problem was selection of suitable high-temperature materials, particularly of the active transducer material. All magnetostrictive transducer materials lose their active properties above their Curie temperature. A transducer material must be used which has a Curie temperature above the maximum desired operating temperature and then it must be incorporated in a probe design which will withstand and operate in the required high-temperature, high-pressure, radioactive environment.

Figure VI-1 is a drawing showing the internal construction of the probe. The housing is of stainless steel and is made in two parts. The lower portion includes the sensitive face which is a resonant diaphragm, 0.254 cm thick. The ferrite tube transducer is attached to the center of this diaphragm, as shown. This tube must be straight and attached at right angles to the center of the diaphragm. Ceramic cement is used to attach the ferrite tube to the diaphragm. This cement can withstand temperatures to 1090°C. The upper portion of the sensor housing contains the electrical coil and ferrite shield. The upper and lower portions of the stainless steel housing are then welded together.

The electrical coil consists of 600 turns of nickel wire wound on a removable coil form. Ceramic cement is applied to the coil after winding to hold it in shape when the form is removed.

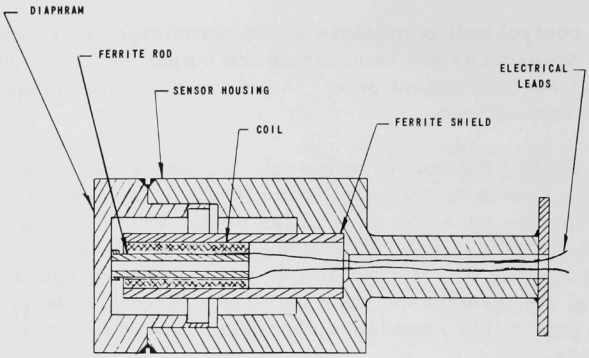


Fig. VI-1

Sectional View of Acoustic High Temperature Sensor Model 120153

The shield consists of a ferrite cylinder of the same type used for the transducer. It is secured, by means of the ceramic cement, into a machined recess in the upper portion of the housing. The coil is cemented into the shield and must be exactly centered by means of a jig while the cement is being fully cured. The coil is positioned so that its lower end coincides with the lower end of the shield.

The probe is designed to be mounted by a clamp which should contact only the extreme upper portion of the housing. The sensor can operate at temperatures up to 480°C and pressures up to 170 atm.

C. Thermal Conductance Probe (Heated Termocouple)

The thermal conductance probe senses level by discriminating between the thermal conductivities of the liquid and vapor phases. The probe consists of a heater and a thermocouple enclosed in a swaged, inorganic insulated, tube as shown in Figure VI-2.

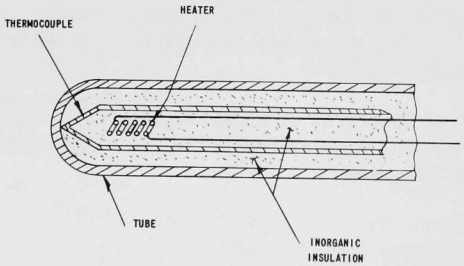


Fig. VI-2

Thermal Conductance Probe

With a constant voltage applied to the heater, the output signal from the thermocouple depends upon the temperature necessary to dissipate the resulting heat to the environment. In the vapor phase, the probe temperature rises above ambient to the point where heat transfer equals heat input. In the liquid phase, the heat transfer is more efficient and a lower probe temperature results. This probe can, therefore, be calibrated to yield the steam-water interface level.

Such a probe has the following advantages over other possible level devices:

1. It is independent of density.
2. It is mechanically rugged.
3. It is inexpensive.
4. It is adaptable to the in-core environment.
5. The output signal is electrical.

D. Differential Pressure Method

Static pressure taps can be used to determine the steam-water interface level inside the reactor vessel. Figure VI-3 shows such an arrangement.

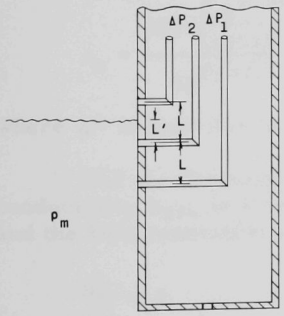


Fig. VI-3

Static Pressure Taps for Determining the Steam-Water Interface Level

From Equation (IV.16):

$$10{,}332\ \Delta P_1 = (\rho_L - \rho_m)L$$

and

$$10{,}332\ \Delta P_2 = (\rho_L - \rho_g)L - (\rho_m - \rho_g)L' \qquad \text{(VI.1)}$$

$$L' = L\frac{[\rho_L - 10{,}332\ (\Delta P_2/L) - \rho_g]}{[\rho_L - 10{,}332\ (\Delta P_1/L) - \rho_g]} \qquad \text{(VI.2)}$$

The only assumption made in determining the interface level is that the mean mixture density, $\rho_m$, does not change between adjacent pressure taps. If only one set of taps would have been installed, this mean mixture density would be unknown and the interface level could not be determined.

E. Nomenclature

| | |
|---|---|
| L | Distance between pressure taps (meters) |
| L' | Interface height above tap 2 (meters) |
| $\rho_g$ | Dry saturated vapor density (kg/cubic meter) |
| $\rho_L$ | Liquid density in legs 1, 2, and 3 (kg/cubic meter) |
| $\rho_m$ | Mean mixture density (kg/cubic meter) |
| $\Delta P_1$ | Differential pressure between taps 1 and 2 (atm) |
| $\Delta P_2$ | Differential pressure between taps 2 and 3 (atm) |

# VII. FUEL PLATE HEAT FLUX AND POWER DISTRIBUTION

If the axial centerline temperature distribution of a fuel plate can be measured, the heat flux distribution and the power generated in this fuel plate can be determined. This temperature is best measured if there exists a "dead" or nongenerating region at the center of the fuel so that the temperature gradient is essentially zero. Thermocouples will be used for this temperature measurement in EBWR and will be squeezed very tightly between two standard thin fuel plates. This "sandwich" arrangement provides the desirable "dead" region on both sides of the thermocouples, as shown in Figure VII-1.

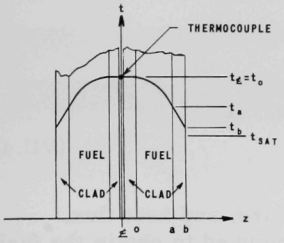


Fig. VII-1

Diagram of Special EBWR Fuel Plate

It is assumed in the following derivation that all the heat conduction is in the z direction, that the heat is uniformly generated, and that the boiling heat flux can be described by the Jens-Lottes type of equation.

For the boiling region where $b < z$,

$$t_b = \frac{250\left(\frac{q''}{3154}\right)^{0.25}}{9e^{P/61.2}} + t_{sat} \qquad \text{(VII.1)}$$

where q" is heat flux in kw/sq m.

For the Zircaloy-2-clad region, where $a < z < b$, the thermal conductivity $k_{zr2}$ is a constant over the temperature range of interest and the heat generation is zero, so that

$$\frac{d^2t}{dz^2} = 0 \quad .$$

Therefore,

$$t_a = t_b + \frac{q''(b-a)}{k_{zr2}} \quad . \qquad \text{(VII.2)}$$

For the fuel region where $0 < z < a$, the thermal conductivity of the uranium, 1.5% niobium, 5% zirconium alloy can be approximated by $k_u = k_{u0} + \sigma_t$ over the temperature range of interest and

$$\frac{d}{dz}\left(k\frac{dt}{dz}\right) + \frac{q''}{a} = 0 \quad .$$

Therefore,

$$t_0 = \frac{-k_{u0}}{\sigma} + \sqrt{\left(t_a + \frac{k_{u0}}{\sigma}\right)^2 + \frac{q''a}{\sigma}} \quad . \tag{VII.3}$$

For the dead-zone region, in which

$$z_{\mathfrak{C}} < x < 0 \quad ,$$

then

$$t_{\mathfrak{C}} = t_0 \quad . \tag{VII.4}$$

For a given fuel plate configuration, system pressure, and heat flux, Equations (VII.1), (VII.2), (VII.3), and (VII.4) can be used to obtain the fuel plate centerline temperature. Selecting a constant system pressure, and a range of heat fluxes, a curve of centerline fuel temperature as a function of heat flux can be obtained. This curve for the special EBWR fuel plate operating in a 41.8-atm system is shown in Figure VII-2. From this curve, the local heat flux can be determined for any measured centerline temperature. The power generated in the fuel plate can be obtained by integrating the heat flux distribution curve.

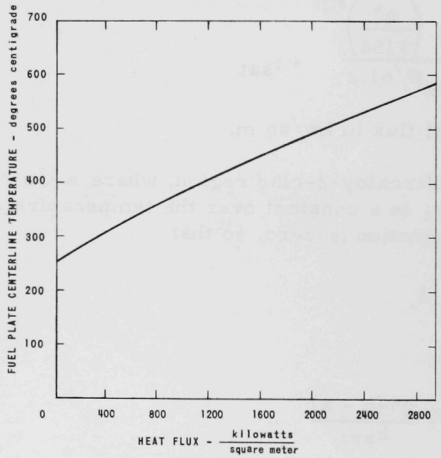


Fig. VII-2

Special Fuel Plate Centerline Temperature as a Function of Local Heat Flux When Operating in a 41.8-Atmosphere System

Because 80 thermocouples spaced at about 1.25-cm intervals along the 122-cm fuel plate are to be used to measure the heat flux distribution, it was decided that a full-scale model of this special fuel plate should be built to test the feasibility of its fabrication. This model fuel plate is shown in Figure VII-3.

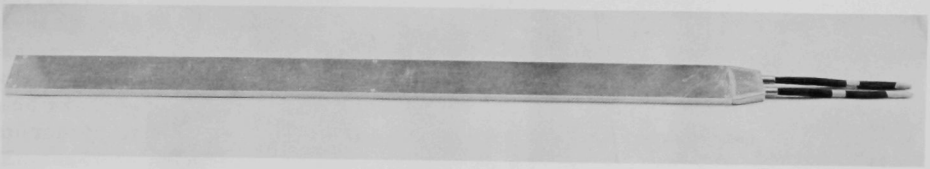

Fig. VII-3

Model Fuel Plate

Figure VII-4 shows the thermocouples spaced at 1.25 cm and Figure VII-5 shows them cemented together with ceramic cement.

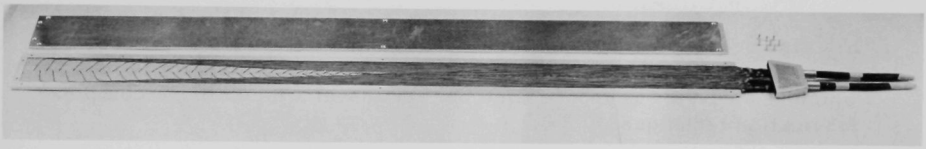

Fig. VII-4

Installation of Thermocouples in Model Fuel Plate

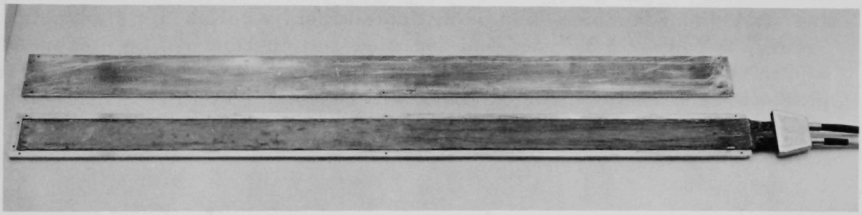

Fig. VII-5

Thermocouples Cemented Together in Model Fuel Plate

It was found that the entire thermocouple wire assembly could be withdrawn and inserted from the top end of the fuel plate, as shown in Figure VII-6. With this type of construction, it would be possible to fabricate the fuel plate and then later insert the thermocouples.

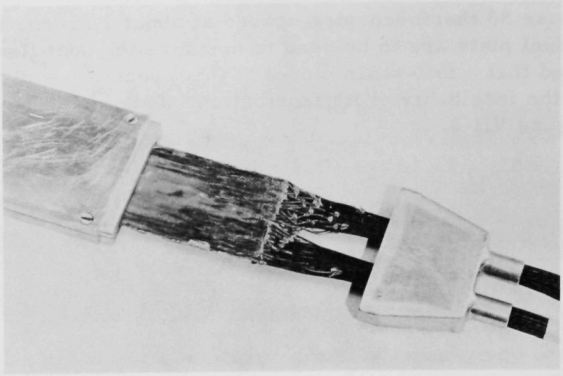

Fig. VII-6

Installation of the Thermocouple Wire Assembly
Through the End of the Model Fuel Plate

An alternative procedure for the attachment of the thermocouples has also been developed. With this design, the thermocouple wires are resistance welded to the fuel plate clad. This produces a thermocouple which has a faster response time but results in a much more complex fabrication technique.

It must also be pointed out that this special fuel plate will not be typical of the other fuel plates in this element nor will the fuel element be typical of other elements in the core. However, a great deal of useful information will be gained from this experiment. First, the thermocouples and attachment technique can be evaluated from a reliability standpoint. Second, the power generated and heat flux distribution will be measured. And third, by precalculating the expected power and heat flux distribution in this special fuel element, a check will be obtained on the validity of these calculation procedures.

## ACKNOWLEDGMENTS

The author would like to gratefully acknowledge the discussions with and valuable suggestions made by W. C. Lipinski, A. Hirsch, P. A. Lottes, and M. Petrick during the preparation of these lectures. My special thanks to V. Kolba who designed the instrumented fuel assemblies; to M. Glass, E. Gunchin, J. O'Grady, and D. Quinn, who assisted in the building of the experimental equipment and the taking of the experimental data; to R. Weinert, who performed the theoretical and experimental study of the hot wire anemometer; and to all the members of both the Reactor Control and Instrumentation and Heat Engineering Sections for their general assistance.